

Identification and Utilization of a Chemical Probe to Interrogate the Roles of PIKfyve in the Lifecycle of β -CoronavirusesDavid H. Drewry,[○] Frances M. Potjeyd,[○] Armin Bayati, Jeffery L. Smith, Rebekah J. Dickmader, Stefanie Howell, Sharon Taft-Benz, Sophia M. Min, Mohammad Anwar Hossain, Mark Heise, Peter S. McPherson, Nathaniel J. Moorman, and Alison D. Axtman*Cite This: *J. Med. Chem.* 2022, 65, 12860–12882

Read Online

ACCESS |



Metrics & More

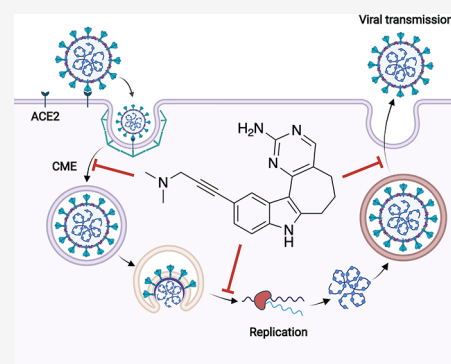


Article Recommendations



Supporting Information

ABSTRACT: From a designed library of indolyl pyrimidinamines, we identified a highly potent and cell-active chemical probe (17) that inhibits phosphatidylinositol-3-phosphate 5-kinase (PIKfyve). Comprehensive evaluation of inhibitor selectivity confirmed that this PIKfyve probe demonstrates excellent kinome-wide selectivity. A structurally related indolyl pyrimidinamine (30) was characterized as a negative control that lacks PIKfyve inhibitory activity and exhibits exquisite selectivity when profiled broadly. Chemical probe 17 disrupts multiple phases of the lifecycle of β -coronaviruses: viral replication and viral entry. The diverse antiviral roles of PIKfyve have not been previously probed comprehensively in a single study or using the same compound set. Our scaffold is a distinct chemotype that lacks the canonical morpholine hinge-binder of classical lipid kinase inhibitors and has a non-overlapping kinase off-target profile with known PIKfyve inhibitors. Our chemical probe set can be used by the community to further characterize the role of PIKfyve in virology.



INTRODUCTION

Phosphatidylinositol-3-phosphate 5-kinase (PIKfyve) is a ubiquitously expressed FYVE finger-containing phosphoinositide kinase that is classified as a lipid kinase. PIKfyve plays diverse roles in membrane trafficking, endosomal transport, GLUT4 translocation, retroviral budding, Toll-like receptor (TLR) signaling, and lysosomal function among others.^{1–3} PIKfyve binds to and phosphorylates the D-5 position of phosphatidylinositol-3-phosphate (PI(3)P) via its FYVE domain to yield phosphatidylinositol-3,5-bisphosphate (PI(3,5)P₂) and phosphatidylinositol 5-phosphate (PI(5)P).¹ The essentiality of PIKfyve is supported by the fact that in multicellular organisms, genetically impaired function of this kinase or its partner proteins that regulate PI(3,5)P₂ homeostasis results in severe disorders, including embryonic/perinatal death.¹

Several inhibitors of PIKfyve have been published with variable potency in cells and selectivity profiling that have been used to define its cellular roles. PIKfyve has been characterized as a critical player in TLR signaling using apilimod as a tool compound (Figure 1). Kinome-wide profiling of apilimod at 1 μ M revealed it to be an exquisitely selective inhibitor of PIKfyve. Furthermore, it was found to have a $K_d = 75$ pM in the DiscoverX PIKfyve binding assay.² Based on its potent inhibition of IL-12 and IL-23, apilimod has been evaluated in clinical trials for Crohn's disease and rheumatoid arthritis.^{4,5} Apilimod inhibits IL-12 and IL-23 through binding to PIKfyve and blocking its phosphotransferase activity.³ It has also been

touted as a treatment for B-cell non-Hodgkin lymphoma (B-NHL) based on its broad anticancer activity *in vitro* and *in vivo* across all subtypes of B-NHL without toxicity to normal cells. It was proposed that the B-NHL cytotoxicity elicited by apilimod results from its disruption of lysosomal function due to PIKfyve inhibition. More recently, apilimod was investigated in clinical trials for the treatment of COVID-19. The proposed antiviral mechanism of apilimod is prevention of viral invasion via inhibition of host cell proteases.⁶ Apilimod was also used to demonstrate that PIKfyve inhibition prevents viral infection by Zaire ebolavirus and SARS-CoV-2 by preventing release of the viral contents from endosomes.⁷

The ability to inhibit retroviral replication and in insulin activation of GLUT4 surface translocation and glucose influx via targeting PIKfyve was confirmed using YM201636 (Figure 1).⁸ In addition, YM201636 inhibits the proliferation of liver cancer cells and tumor growth in a murine hepatic cancer model. The proposed mechanism via which it inhibits tumor growth is through promoting EGFR expression, which induces autophagy.⁹ Dysregulation of autophagy by YM201636 and resultant cell death have been observed in other cell types as well.¹⁰

Received: May 2, 2022

Published: September 16, 2022



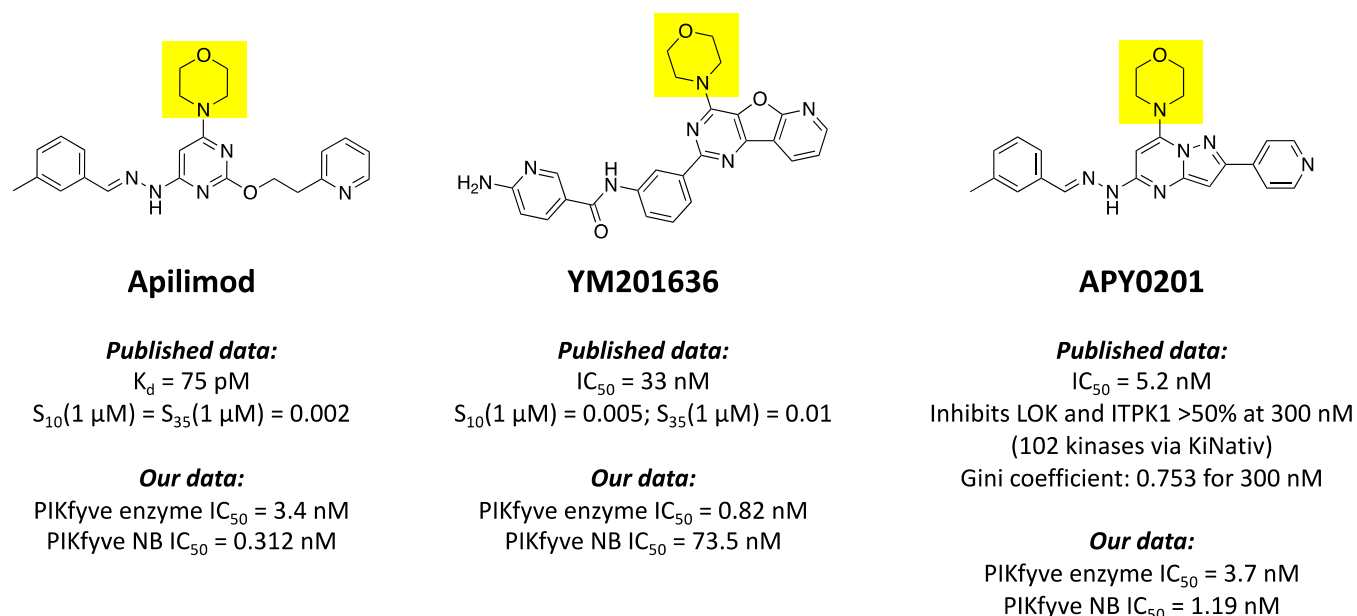


Figure 1. Structures, potency, and selectivity values for published PIKfyve inhibitors. The shared morpholine ring in the three scaffolds is highlighted in yellow.

Finally, YM201636 reversibly impairs endosomal trafficking in NIH3T3 murine cells.¹¹ YM201636 is a potent inhibitor of PIKfyve ($IC_{50} = 33 \text{ nM}$) and the recently disclosed kinome-wide selectivity of YM201636 (Figure 1) confirmed it as a very selective inhibitor of PIKfyve.¹²

Finally, APY0201 is a PIKfyve inhibitor that has demonstrated broad antimultiple myeloma activity.¹³ APY0201 upregulated genes in the lysosomal pathway, increased cellular vacuolization, and activated the transcription factor EB, a master regulator of lysosomal biogenesis and autophagy.¹³ Like apilimod, APY0201 was used to confirm the function of PIKfyve in the IL-12/23 production pathway and in inflammatory disease pathologies driven by these interleukins.¹⁴ In situ native kinase profiling (KiNativ) using an ATP-competitive probe and Jurkat cell lysate was used to determine the selectivity of APY0201 for 24 human lipid kinases and 83 human protein kinases. This selectivity screening at 300 nM revealed >50% inhibition of LOK and ITPK1 and allowed calculation of a Gini coefficient of 0.753. APY0201 was also profiled versus apilimod against a panel of 137 G protein-coupled receptors (GPCRs), enzymes, ion channels, and transporters and found to demonstrate negligible inhibition relative to its IC_{50} value in the PIKfyve kinase assay (5.2 nM). Apilimod, by comparison, demonstrated inhibitory activity on some GPCRs.¹⁴

ATP-competitive phosphatidylinositol-3-kinase (PI3K) and phosphatidylinositol-3-kinase-related kinase (PIKK) inhibitors have historically possessed a critical morpholine that forms a hydrogen bond with the kinase hinge region.¹⁵ Apilimod, YM201636, and APY0201 bear this morpholine (boxed in Figure 1).¹⁴ For YM201636, one of the off-target kinases that potently binds (percent of control (PoC) = 9.8 at $1 \mu\text{M}$) is a catalytic subunit of PI3Ks, PIK3CB.¹² Structural studies around PIKfyve have been limited. All Protein Data Bank entries related to PIKfyve were generated using medium–low resolution Cryo-EM (5.1–6.6 Å). These structures reveal that PIKfyve exists as a complex with five copies of a scaffolding protein known as Vac14. Furthermore, associated models suggest that while this heteroprotein complex interacts with the membrane, the

PIKfyve active site is rotated such that it cannot access membrane-incorporated phosphoinositides.¹⁶

Here, we present a potent and selective PIKfyve inhibitor that lacks the hinge-binding morpholine of other published inhibitors. Without the presence of morpholine, our off-target kinase profile does not contain other lipid kinases and is non-overlapping with that of known PIKfyve inhibitors. Medicinal chemistry optimization of the indolyl pyrimidinamine scaffold was enabled by a PIKfyve cellular target engagement assay in tandem with kinome-wide selectivity screening. Our chemical probe (17) was evaluated alongside its structurally related negative control (30) and published PIKfyve inhibitors to confirm the role of PIKfyve in mediating several pathways that viruses depend upon for entry, replication, and transmission.

RESULTS AND DISCUSSION

Rationale for the Selection of the Parent Inhibitor. To enable illumination of the function of understudied kinases, we identify and synthesize analogues of published scaffolds that inhibit poorly characterized kinases. AMG28 (Figure 2) was selected based on data provided for it in the MRC Kinase Profiling Inhibitor Database. One method by which we define a kinase as understudied is via publication count. If we set a threshold of 100 publications on the human form of a particular kinase, nearly 65% of the kinases targeted by AMG28 with <20% activity remaining at the $1 \mu\text{M}$ screening concentration meet this criterion. While the MRC profiling data provided insight into the activity of this compound, the panel is only comprised of 140 wild-type (WT) human kinases. Motivated by its inhibition profile and with a desire to screen it in a more comprehensive kinase panel, we first remade AMG28.

Once synthesized, AMG28 was screened against the DiscoverX scanMAX platform at $1 \mu\text{M}$. This panel includes 403 WT human kinases and thus greatly expands the data generated for AMG28 versus that from MRC. AMG28 demonstrated PoC < 10 for 20 WT human kinases, translating to an adjusted selectivity score of $S_{10}(1 \mu\text{M}) = 0.05$. When screened at the same concentration ($1 \mu\text{M}$), several kinases

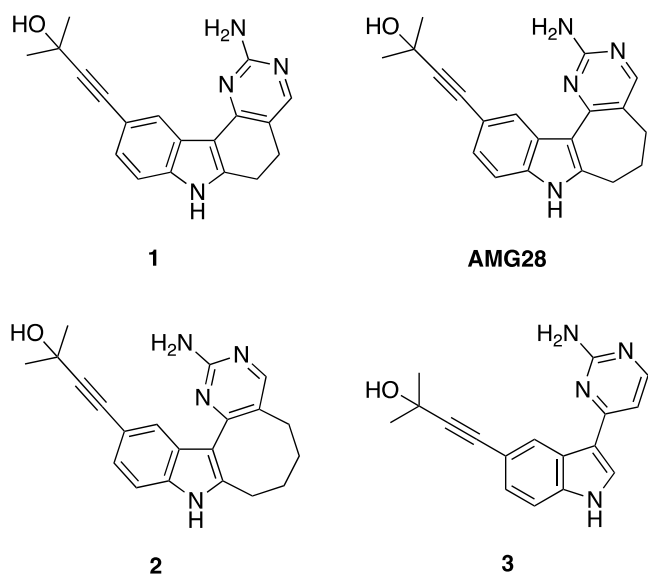


Figure 2. Structures of analogues 1–3 and AMG28.

showed low activity remaining in both kinase panels (Figure 3A). Beyond these kinases in common, PIKfyve was identified as a kinase of interest based on its PoC < 1. Enzymatic follow-up in dose–response using commercially available assays was pursued for selected understudied kinases and family members identified in the two large panel screening efforts (MRC and DiscoverX). Part of this effort involved working with SignalChem to establish a PIKfyve enzyme inhibition assay using their commercially available protein. As shown in Figure 3B, AMG28 was validated as an efficacious inhibitor of most of the kinases selected and, notably, the PIKfyve PoC value was confirmed to translate to potent inhibition of PIKfyve enzymatic activity ($IC_{50} = 2.2$ nM). The narrow kinome-wide selectivity of AMG28 against 403 WT human kinases coupled with validated inhibition of under-

studied kinases in an orthogonal enzymatic format encouraged us to pursue structural diversification via analogue synthesis.

Exploring the Role of the Seven-Membered Ring. We began our campaign with a subset of indolyl pyrimidinamine analogues that probed the importance of the seven-membered ring system in AMG28. There are no high-resolution or cocrystal structures of PIKfyve. Our own kinase inhibitor design experience and work of others in the field have confirmed the aminopyrimidine as a common hinge-binding motif.^{17–20} Although they involve an unrelated human protein kinase that shares only 21% sequence identity with PIKfyve, recently solved cocrystal structures of AMG28 bound to TTBK1 (PDB: 7JXX and 7ZHN) demonstrate that the aminopyrimidine ring in AMG28 makes essential hydrogen bonds with the hinge of TTBK1.^{21,22} These studies suggest that aminopyrimidine could also bind the hinge of PIKfyve. It was suggested by the authors of the Biogen TTBK1 paper that the three methylene groups of the seven-membered ring help maintain the planarity of the molecule rather than making key contacts with the protein.²¹ To explore and support these hypotheses as they relate to PIKfyve, we both augmented and decreased the number of methylene groups in the saturated ring system to yield the corresponding six- and eight-membered analogues of AMG28 (1 and 2, respectively, in Figure 2). Furthermore, we made the ring-opened analogue of AMG28 (3, Figure 2). We sent these analogues to DiscoverX for kinome-wide profiling to determine how their PIKfyve PoC values and selectivity compared with AMG28. The DiscoverX scanMAX results for these compounds and AMG28 are summarized in Table 1. We confirmed the PIKfyve PoC values using the orthogonal PIKfyve enzymatic assay at SignalChem. Analogues from Table 1 plus the published PIKfyve inhibitors included in Figure 1 were evaluated. Once the PoC values were validated via the enzymatic assay, we established a PIKfyve cellular target engagement (NanoBRET, NB) assay to support medicinal chemistry optimization of PIKfyve inhibitors. We and others have found that using the

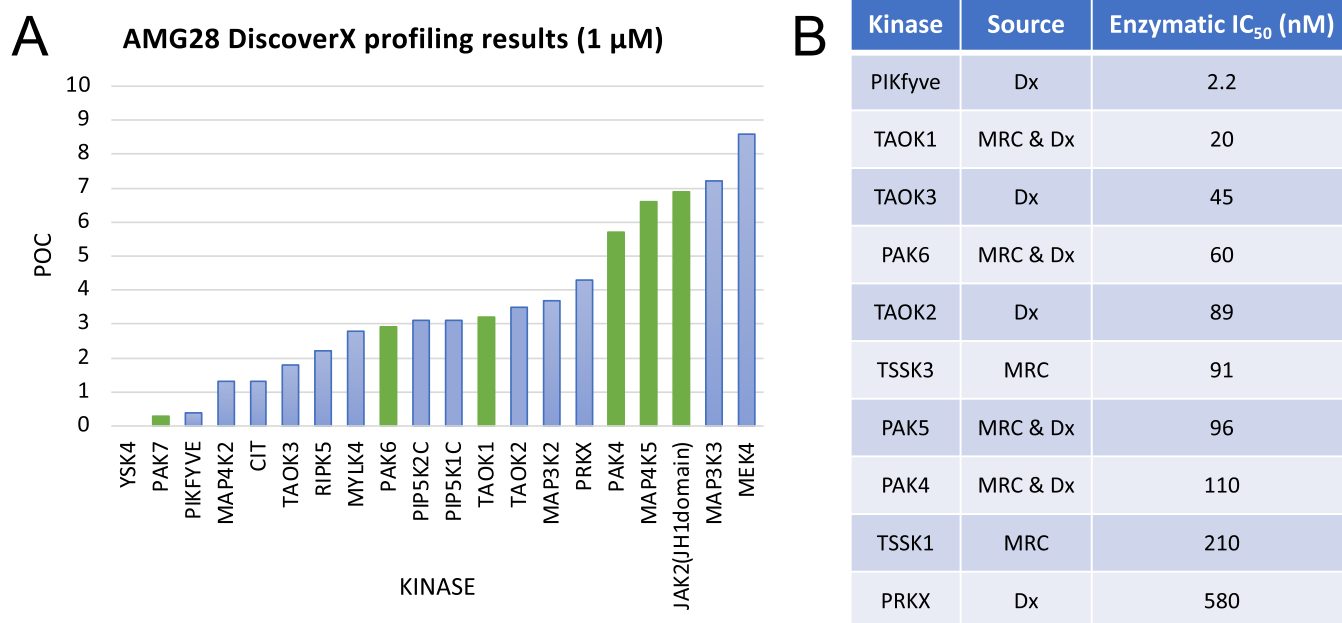


Figure 3. AMG28 is a kinase inhibitor with narrow kinome-wide selectivity. (A) AMG28 DiscoverX screening results for kinases with <10 percent of control (POC) remaining when screened at 1 μ M. Kinases common to the MRC panel are represented as green bars. (B) Selective enzymatic follow-up IC_{50} values for understudied kinases and family members identified via the DiscoverX (Dx) and/or MRC screening campaigns.

Table 1. PIKfyve and Selectivity Data for Ring Modification Library and Published Inhibitors^{2,12}

compound	PIKfyve PoC ^a	PIKfyve enzymatic IC ₅₀ (nM)	PIKfyve NB IC ₅₀ (nM)	S ₁₀ (1 μM) ^b	# scanMAX kinases with PoC < 10 ^c
1	0	NT ^d	220	0.05	20
AMG28	0.4	2.2	14.1	0.052	21
2	3.4	61	2450	0.007	3
3	0	6.1	21.1	0.084	34
Apilimod	NT	3.4	0.312	0.002	1
YM201636	0	0.82	73.5	0.005	2
APY0201	NT	3.7	1.19	NT	NT

^aPercent of control (PoC) values determined at 1 μM via DiscoverX scanMAX profiling. ^bS₁₀(1 μM): percentage of screened kinases with PoC < 10 at 1 μM. ^cNumber of kinases with PoC < 10 at 1 μM. ^dNT: not tested.

NanoBRET assay to drive the analogue design provides a useful and relevant measure of cell affinity for the kinase of interest that also takes into account the ability of compounds to enter cells. All compounds in Table 1 as well as the published PIKfyve inhibitors in Figure 1 were tested in the PIKfyve NanoBRET assay. This first compound set demonstrated that opening the ring to yield analogue 3 did not result in improved PIKfyve potency versus parent AMG28 and caused a loss in kinome-wide selectivity. Analogue 1 maintained the kinome-wide selectivity and potency of AMG28, indicating that a six-membered ring is tolerated by PIKfyve. Finally, expansion to the eight-membered ring produced compound 2 that did not bind with high affinity to PIKfyve or many other kinases in the larger kinome. This small compound set showed that compounds bearing six- and seven-membered rings were effective inhibitors of PIKfyve but require improvement of kinome-wide selectivity to be useful tool compounds. In contrast, incorporation of an eight-membered ring was viewed as a mechanism via which to access highly selective compounds that lack PIKfyve activity.

Probing the Importance and Nature of the Alkyne.

Next, we prepared several compounds to solidify our understanding of the importance of ring size, while simultaneously determining the tolerance of PIKfyve to modification of the

alkyne portion of AMG28. First, we synthesized matched sets of analogues bearing six-, seven-, and eight-membered rings with the alkyne portion of modified AMG28. The first subset of these compounds (4–6) incorporated modest changes to the terminal alkyne. Through modifying the substituted propargylic alcohol in AMG28 to an alkyne bearing a pyridine, we probed the space in the PIKfyve binding pocket typically occupied by the alkyne. We hypothesized that fewer kinases would tolerate additional bulk on the terminus of the alkyne. Next, we made a matched set of analogues (7–9) in which the alkyne was removed and a para-fluorobenzene ring directly attached in its place. These analogues were designed to determine the importance of the alkyne as well as the affinity of PIKfyve for this biaryl system with a very different shape. Analogues 7–9 will fill a substantially different volume in the kinase ATP site versus those bearing an alkyne.

To evaluate these analogues versus those in Table 1, we first sent them for kinome-wide profiling in the DiscoverX scanMAX panel. All analogues in Table 2 demonstrated improved selectivity scores versus AMG28. In the case of analogues 4 and 6, this reduced the binding affinity exhibited for many kinases across the kinome, echoed by a drastic decrease in PIKfyve activity. Seven-membered analogue 5, in contrast, was confirmed by three orthogonal assays to bind to PIKfyve and result in the inhibition of the enzyme, but it was significantly less active than AMG28. Overall, the pyridyl-bearing alkyne did not result in an improvement of PIKfyve inhibition, which suggested that an aryl ring on the alkyne terminus was not well tolerated by this kinase. Analogues 7–9 also had improved kinome-wide selectivity (all S₁₀(1 μM) values < 0.01) and for compounds 7 and 8, this was not coupled with substantial losses in PIKfyve affinity. One interesting difference between analogues 7 and 8 was observed when comparing their PIKfyve enzymatic and NanoBRET assay IC₅₀ values (Table 2). Despite their structural similarity, for analogue 7, there was a more significant drop-off in potency when moving from the PIKfyve enzymatic assay to the PIKfyve NanoBRET assay.

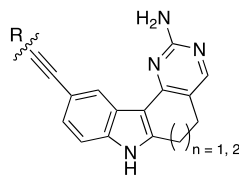
PIKfyve will tolerate alkyne removal. Once again, the seven-membered analogue (8) was the most potent PIKfyve inhibitor from this subset. Based on its potency, which was confirmed in

Table 2. PIKfyve and Selectivity Data for Alkyne Modification Library

compound	n	R	PIKfyve PoC ^a	PIKfyve enzymatic IC ₅₀ (nM)	PIKfyve NB IC ₅₀ (nM)	S ₁₀ (1 μM) ^b	# scanMAX kinases with PoC < 10 ^c
4	1	A	69	NT ^d	2980	0.002	1
5	2	A	12	22	885	0.012	5
6	3	A	100	580	5290	0	0
7	1	B	0.3	8.2	380	0.007	3
8	2	B	0	9.3	11.4	0.005	2
9	3	B	37	NT	2560	0.005	2
10	1	C	0.9	NT	1170	0.027	11
11	2	C	0	NT	45.7	0.016	7
12	1	D	2.3	34	4970	0.017	7
13	2	D	2.2	26	1560	0.02	8

^aPercent of control (PoC) values determined at 1 μM via DiscoverX scanMAX profiling. ^bS₁₀(1 μM): percentage of screened kinases with PoC < 10 at 1 μM. ^cNumber of kinases with PoC < 10 at 1 μM. ^dNT: not tested.

Table 3. PIKfyve and Selectivity Data for Alkyne Optimization Library



Compound	n	R	PIKfyve PoC ^[a]	PIKfyve enzymatic IC ₅₀ (nM)	PIKfyve NB IC ₅₀ (nM)	S ₁₀ (1 μM) ^[b]	# scanMAX kinases with PoC <10 ^[c]
14	1		28	77	>10000	0.015	6
15	1		0.3	NT ^[d]	300	0.015	6
16	1		0	NT	123	0.015	6
17	2		0.1	6.9	4.01	0.02	8
18	2		91	NT	>10000	0.017	7
19	2		99	140	1600	0	0
20	2		0.5	6.2	314	0.027	11
21	2		0	NT	4.05	0.122	49
22	2		1	NT	40	0.084	34
23	2		8.7	NT	2160	0.027	11
24	2		1.1	NT	290	0.035	14
25	2		0	1.9	9.65	0.055	22
26	2		0	1.8	12.7	0.017	7

^aPercent of control (PoC) values determined at 1 μM via DiscoverX scanMAX profiling. ^bS₁₀(1 μM): percentage of screened kinases with PoC < 10 at 1 μM. ^cNumber of kinases with PoC < 10 at 1 μM. ^dNT: not tested.

the PIKfyve enzyme assay, and selectivity (Figure S1B), compound **8** was considered a PIKfyve chemical probe candidate in need of additional characterization. Considering these initial matched sets (4–9) together, the seven-membered ring represents a sweet spot in terms of providing potent PIKfyve inhibition, while the six-membered ring still maintains some potency. These two ring sizes provide analogues with similar selectivity scores when profiled broadly. In contrast, the eight-membered ring is suboptimal for PIKfyve potency but does improve kinome-wide selectivity, suggesting that few kinases tolerate its inclusion.

Another two matched pairs of analogues bearing six- and seven-membered rings were prepared via modifying the alkyne portion of AMG28. These compounds were designed to incorporate the more favorable ring sizes (six and seven) and

explore the impact of a more subtle change to the substituted propargylic alcohol of AMG28 (**10** and **11**) or to the biaryl system of analogues **7–9** (**12** and **13**). Analogues **10** and **11** were designed to modify the steric bulk directly attached to the carbon bearing the propargylic alcohol. Analogues **12** and **13** were designed to incorporate a smaller 1-methylpyrazole ring system with a different electronic character in place of the para-fluorobenzene. Based on our other analogues, we hypothesized that these changes would be tolerated by PIKfyve and result in potent inhibitors but with unknown kinome-wide selectivity.

Evaluation of analogues **10–13** in the DiscoverX scanMAX panel revealed them to have promising selectivity against the larger kinome. These compounds had selectivity scores that fall between their six- and seven-membered comparators in Tables 1 (1 and AMG28) and 2 (4, 5, 7, and 8). Comparing the modified

propargylic alcohols (**1**, AMG28, **10**, and **11**) with the pyridine-bearing alkynes highlighted that these smaller groups at the terminus of the alkyne are better tolerated by PIKfyve. In comparing the biaryl systems, those analogues bearing a para-fluorobenzene (**7** and **8**) were more potent PIKfyve inhibitors than those with a 1-methylpyrazole (**12** and **13**). Once again, the seven-membered analogues (**11** and **13**) outperformed their six-membered congeners (**10** and **12**) in terms of PIKfyve potency. This larger data set (Tables 1 and 2) allowed us to consider the correlations of PIKfyve PoC, enzymatic, and NanoBRET data. Good agreement was found between the two biochemical methods, while some variation was observed in moving into the cell-based assay. Generally, a loss in potency was noted in the NanoBRET assay, a common finding when one moves from a biochemical assay to a cellular context. This is one reason we value the use of this cellular target engagement assay to support optimization, as it identifies compounds with most promise for robust cellular activity.

Diversifying the Terminal Alkyne. Next, we synthesized several indolyl pyrimidinamines to probe the tolerance of PIKfyve to modification of the alkyne terminus for analogues bearing six- or seven-membered rings. Based on the analogues in Tables 1 and 2, we made a small set of six-membered derivatives bearing an alkyne capped with diverse groups. We designed these to include a five-membered 1-methylimidazole (**14**), a cyclopropyl ring (**15**), or a dimethylamino group (**16**). These substituents represent diversity in size and electronic nature, exploring the size of a ring system tolerated within this portion of the PIKfyve binding pocket as well as nitrogen atoms projected in various directions. They were designed to expand on what we learned from pyridine-bearing analogue **4** and propargylic alcohol analogue **10**: smaller groups at the alkyne terminus are better tolerated by PIKfyve. These new analogues aimed to probe whether the hydroxyl group is essential for potent PIKfyve inhibition. We hypothesized that a smaller group on the alkyne terminus would be better tolerated versus the appended aryl system.

When analogues **14–16** were broadly profiled via the DiscoverX *scanMAX* panel, they demonstrated good selectivity scores and all three bound potently to only 6 of 403 WT human kinases at 1 μM . This places them in the same selectivity range as other six-membered analogues from Tables 1 and 2, which bind 1–20 WT human kinases in the same panel. The PIKfyve potency of these compounds was found to be poor for 1-methylimidazole-bearing analogue **14** but improves when this ring system was replaced with the smaller cyclopropyl (**15**) or dimethylamino (**16**) groups. The DiscoverX PIKfyve PoC data was found to correlate well with the PIKfyve NanoBRET assay IC_{50} values for these analogues. Since they did not improve on the potency and selectivity of probe candidate **8**, enzymatic confirmation for analogues **15** and **16** was not pursued. The inactivity of analogue **14** in the PIKfyve NanoBRET assay prompted its evaluation in the PIKfyve enzymatic assay. Its IC_{50} value in the PIKfyve enzymatic assay suggests that this scaffold, like pyridyl-bearing analogues **6** and **7**, suffers from a 40–70-fold loss in potency when moving from the biochemical to the cell-based assay system. All data for **14–16** are summarized in Table 3.

Since moving from the six- to seven-membered system was accompanied by gains in PIKfyve potency (**1** versus AMG28, **4** versus **5**, **7** versus **8**, **10** versus **11**, and **12** versus **13**), the attachment of the dimethylamino group to the seven-membered core as well as further exploration of the tolerance of PIKfyve to

amine-bearing substitution was planned. The seven-membered equivalent of **16** was prepared (**17**) as well as analogues of AMG28 with the hydroxyl group replaced with an acyl amine (**18**) or a sulfonamide (**19**).

Furthermore, we designed additional propargylic alcohol analogues since their potency was still optimal versus other alkyne-bearing derivatives (**1**, AMG28, **10**, and **11** versus **4**, **5**, and **14–16**). Compounds were designed to cap the propargylic alcohol of AMG28 with a methyl group (**20**) and reduce the bulk on the carbon to which the alcohol is attached (**21**). Next, three analogues that project the alcohol further into the PIKfyve binding pocket via insertion of a methylene group were selected without bulk (**22**), with maintained substitution of AMG28 (**23**), and with a sterically hindered alcohol (**24**). Finally, two derivatives with increased bulk around the carbon bearing the propargylic alcohol were prepared, one with methyl, ethyl substitution (**25**) and another with diethyl substitution (**26**). We hypothesized that reducing the bulk around the propargylic alcohol (**21** and **22**) would result in analogues that were better tolerated by many kinases and thus reduce their kinome-wide selectivity. Analogues bearing larger groups on the terminus of the alkyne (**4** and **5**, for example) suggest that the pocket accommodates bulk. Thus, the propargylic alcohol analogues with a methylene unit insertion between the alkyne terminus and alcohol (**22–24**) or those sterically encumbered around the alcohol (**25** and **26**) were predicted to be well tolerated by PIKfyve. Finally, the dimethylamino analogue (**16**) indicated that the hydroxyl group is dispensable and thus analogue **20** was pursued.

We evaluated each of these analogues (**17–26**) using the DiscoverX *scanMAX* panel and in the PIKfyve NanoBRET assay. The nitrogen-bearing analogues (**17–19**) demonstrated good kinome-wide selectivity, binding with PoC < 10 to nine or fewer WT human kinases at 1 μM . The PIKfyve potency of these compounds, however, ranged in the DiscoverX and NanoBRET assays. Only analogue **17** was active and, given its single-digit potency coupled with kinome-wide selectivity (Figure S1A), it was selected for additional characterization as a PIKfyve probe candidate. The enhanced steric bulk (or alternative functionality) on the alkyne terminus in **18** and **19** was not well tolerated by PIKfyve.

Moving to the propargylic alcohol analogues (**20–26**), the kinome-wide selectivity of these analogues varied widely, and they displayed PoC < 10 for between 7 and 49 kinases at 1 μM . As predicted, the less sterically encumbered analogues **21** and **22** bound the most kinases in the *scanMAX* panel and are more promiscuous compounds than AMG28. For those analogues where steric bulk was added to the carbon center bearing the alcohol, improved selectivity was only observed with the diethyl analogue (**26**). In comparison, analogue **25** (methyl, ethyl derivative) and AMG28 demonstrated comparable $S_{10}(1 \mu\text{M})$ scores. A thorough analysis of analogue **26** was driven by interest in its inhibition of off-target kinases, revealing that analogue **26** lacks the requisite selectivity to be considered as a probe candidate.²² Finally, analogues **20**, **23**, and **24** exhibited intermediate selectivity (11–14 of 403 WT human kinases with PoC < 10 when profiled at 1 μM). All analogues (**20–26**) demonstrated PoC < 10 in the PIKfyve assay included in the DiscoverX *scanMAX* panel. This potency translated to several analogues (**21**, **25**, and **26**) with IC_{50} values < 20 nM in the PIKfyve NanoBRET assay.

Follow-up using the PIKfyve enzyme assay was carried out for several compounds that were potent (IC_{50} < 350 nM) in the

PIKfyve NanoBRET assay. It is worth noting that for analogue **20** there was a larger drop-off in potency when moving from the PIKfyve enzymatic assay to the PIKfyve NanoBRET assay when compared to structurally similar analogues. Despite their orthogonally validated PIKfyve potency, the lack of selectivity of these compounds for PIKfyve when profiled broadly precluded their consideration as PIKfyve chemical probes. In pursuit of a negative control compound to be used alongside a PIKfyve chemical probe, analogue **19** was sent for enzymatic follow-up. A suitable negative control compound should bear structural similarity to the chosen chemical probe but lack potency in the PIKfyve NanoBRET and enzymatic assays and demonstrate favorable kinome-wide selectivity. Despite its impressive $S_{10}(1 \mu\text{M})$ score (Table 3), analogue **19** retained PIKfyve potency and thus was removed from consideration as a negative control compound, highlighting a need for additional analogues. All data for analogues **17–26** are included in Table 3.

Designing a Negative Control. Since a suitable negative control compound had not been identified, we designed analogues that, based on our structure–activity relationships (SAR), would bind few kinases when profiled broadly and lack PIKfyve activity. We wanted to make at least one analogue of our two chemical probe candidates: **8** and **17**. Thus, we designed some analogues bearing an alkyne and one with a biaryl system. Our studies included in Tables 1 and 2 narrowed in on the eight-membered ring as demonstrating both reduced affinity for PIKfyve and for the larger kinome, making it the ideal ring system to use in preparation of our negative control candidates. Given the promising selectivity score of analogues **14–16** ($S_{10}(1 \mu\text{M}) = 0.015$) and the structural similarity of **16** to probe candidate **17**, we first designed the eight-membered analogues of these three compounds. We hypothesized that ring expansion of these analogues would not be tolerated by PIKfyve and that a similar potency trend, albeit reduced, would be maintained as was seen for analogues **14–16**. To complement the structure of probe candidate **8**, we opted to replace the para-fluorobenzene with a smaller cyclopropyl ring and expanded the seven-membered ring to an eight-membered system. We anticipated that moving to the smaller cyclopropyl ring in this position would remove the favorable interactions that the para-fluorobenzene group makes with the PIKfyve binding site. Furthermore, direct attachment of a ring system in analogues **7–9** and **12–13** resulted in favorable kinome-wide selectivity, suggesting that this approach could result in a negative control compound with the requisite selectivity.

Kinome-wide profiling at $1 \mu\text{M}$ was carried out for the four analogues (**27–30**) via the DiscoverX scanMAX platform. All analogues displayed impressive selectivity scores with $\text{PoC} < 10$ for only 2 out of 403 WT human kinases. More variable data were observed when these analogues were tested in the PIKfyve NanoBRET and enzymatic assays. Analogues **28** and **29** maintained potency in the PIKfyve NanoBRET assay, a finding that was confirmed in orthogonal follow-up using the PIKfyve enzyme assay. In comparison, when N-methylimidazole was added to the alkyne terminus to produce analogue **27**, PIKfyve potency in the NanoBRET assay was completely lost. The maintenance of some activity in the PIKfyve enzymatic assay but not in the PIKfyve NanoBRET assay suggests that cell entry could contribute to this loss in activity. Analogue **27** was excluded from consideration as a negative control due to its maintenance of PIKfyve enzymatic inhibition ($\text{IC}_{50} < 300 \text{ nM}$) and potential cell penetrance issues. Moving to analogue **30**, PIKfyve NanoBRET potency was lost and this loss in potency

was echoed in the PIKfyve enzymatic assay ($\text{IC}_{50} > 700 \text{ nM}$). This compound demonstrated the weakest potency of all compounds tested in the PIKfyve enzymatic assay. When we examined the $S_{35}(1 \mu\text{M})$ DiscoverX scanMAX fraction for analogue **30** (Figure S1C), MAST1 was the only WT human kinase included ($\text{PoC} = 32$). Given its excellent kinome-wide selectivity and lack of PIKfyve potency, compound **30** is a good candidate for our negative control compound.

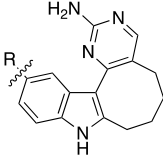
Chemical Probe Selection. To determine whether **8** and **17** meet the chemical probe criteria, we carried out additional enzymatic validation studies to confirm their selectivity criteria.²³ These studies were designed to supplement the DiscoverX scanMAX data through determining whether WT human kinases with $\text{PoC} < 35$ in this panel also displayed potent inhibition when evaluated in the corresponding enzyme or NanoBRET assay (where available). All enzyme assays were executed at the K_m value for ATP for the specific kinase. Based on the data collected, which is included in Table S1, we found that, in addition to PIKfyve, three of the six kinases in the $S_{35}(1 \mu\text{M})$ fraction from the DiscoverX scanMAX panel were potently inhibited or engaged by analogue **8**: MYLK4, PIP5K1C, and PISP4K γ . These three kinases are within 30-fold of the PIKfyve enzymatic and NanoBRET IC_{50} values. Analogue **8** demonstrates >415-fold selectivity over all other kinases evaluated. As an orthogonal screen, a small panel of understudied kinases was selected based on the inhibition data observed for AMG28 in the MRC panel (Figure 3A). No kinase in this panel was inhibited >55% when analogue **8** was screened at $1 \mu\text{M}$ in these enzymatic assays (Table S2), so no further follow-up was carried out.

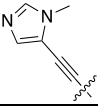

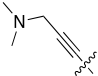

Moving to analogue **17**, enzymatic and/or NanoBRET assays were run for 18 of 20 kinases in the $S_{35}(1 \mu\text{M})$ fraction from the DiscoverX scanMAX panel (Table S3). In addition, the same orthogonal screen of understudied kinases that was executed for analogue **8** was carried out for compound **17** (Table S2). The potent inhibition ($\text{PoC} = 14$) of MAP4K5 at $1 \mu\text{M}$, which was also targeted by AMG28 (Figure 3A), warranted additional enzymatic follow-up (Table S3). Finally, the potency of analogue **8** on PISP4K γ motivated our exploration of the activity of analogue **17** in the PISP4K γ NanoBRET assay. Of the 20 kinases for which we executed orthogonal follow-up, only two kinases in addition to PIKfyve were potently inhibited by analogue **17**: MYLK4 and MAP4K5. These two kinases are within 30-fold of the PIKfyve enzymatic and NanoBRET IC_{50} values. Analogue **17** demonstrates >42-fold selectivity over all other kinases evaluated. The weak binding of compound **17** to MAP4K5 in the DiscoverX scanMAX assay highlights the utility of orthogonal assay formats to confirm the results.

To determine whether the biochemical selectivity profile of analogue **17** was preserved when moving into cells, we ran the MYLK and MAP4K5 NanoBRET assays. The generated NanoBRET IC_{50} values of 265 nM for MYLK and >10 000 nM for MAP4K5 (Table S3) exposed that analogue **17** demonstrates improved selectivity in cells. A 10-fold biochemical selectivity window for PIKfyve versus MYLK4 became a 66-fold window in cells, while the compound was not found to bind to MAP4K5 in cells (Figure S2). Thus, compound **17** appears to be even more selective for PIKfyve when employed in cell-based studies.

The potency of analogue **17** coupled with its selectivity profile makes it the optimal choice as a PIKfyve chemical probe. Analogue **8**, however, is also a high-quality, potent, and selective PIKfyve inhibitor that can be used in parallel, especially given its off-target inhibition profile differs from that of analogue **17**.

Table 4. PIKfyve and Selectivity Data for Compounds Designed as Potential Negative Control Options



Compound	R	PIKfyve PoC ^[a]	PIKfyve enzymatic IC ₅₀ (nM)	PIKfyve NB IC ₅₀ (nM)	S ₁₀ (1 μM) ^[b]	# scanMAX kinases with PoC <10 ^[c]
27		97	290	>10000	0	0
28		9.8	75	700	0.002	1
29		21	430	683	0	0
30		88	720	>10000	0.002	1

^aPercent of control (PoC) values determined at 1 μM via DiscoverX scanMAX profiling. ^bS₁₀(1 μM): percentage of screened kinases with PoC < 10 at 1 μM. ^cNumber of kinases with PoC < 10 at 1 μM.

Before launching into cell-based phenotypic assays, we analyzed the aqueous kinetic solubility and mouse liver microsomal stability of compound 17. While this small molecule was found to have excellent aqueous solubility (109.1 μM), its microsomal stability is suboptimal. After 30 min incubation with mouse liver microsomes, only 12.6% of the compound remained. While this suggests that our chemical probe is not suitable for use *in vivo*, it does not preclude its *in vitro* utility. Studies carried out by Biogen that employed AMG28 as a starting point have led to compounds that are stable *in vivo*.^{21,24} The structural modifications that Biogen made offer suggestions to how additional stability could be imparted into our scaffold.

SAR Observed for Indolyl Pyrimidinamines. In summary, we prepared 30 indolyl pyrimidinamines and remade AMG28. Many of these compounds demonstrate potent affinity for PIKfyve: 22 compounds with PoC < 21 in DiscoverX scanMAX assay when screened at 1 μM. 16 of these 22 demonstrated an IC₅₀ < 400 nM in the PIKfyve NanoBRET assay, confirming that this biochemical binding data translated to binding affinity for PIKfyve in cells. Furthermore, the binding affinity of these compounds was validated in the PIKfyve enzymatic assay, solidifying that these are inhibitors of the PIKfyve function. A correlation between PIKfyve NanoBRET and enzyme data was observed for the indolyl pyrimidinamines such that an enzymatic IC₅₀ value of <10 nM was associated with a NanoBRET IC₅₀ value of <25 nM. With two exceptions (7 and 20), an enzymatic IC₅₀ value of >22 nM resulted in a NanoBRET IC₅₀ value of >680 nM. In addition to PIKfyve potency, several compounds display excellent kinome-wide selectivity. We narrowed in on six- and seven-membered analogues as the most efficacious PIKfyve inhibitors in terms of potency and selectivity and determined that the alkyne is dispensable since a biaryl analogue (8) retained probe-like qualities. In all cases where a matched pair of six- and seven-membered analogues was synthesized (1 and AMG28, 4 and 5, 7 and 8, 10 and 11, 12 and 13, and 16 and 17), the seven-

membered analogue demonstrated enhanced (3–33-fold) PIKfyve NanoBRET affinity.

PIKfyve Inhibition Prevents β-Coronavirus Replication. We next confirmed that the binding affinity and enzymatic inhibition data of our chemical probe translated to a cellular phenotype through evaluation of the activity of our compound series in relevant cellular assays based on ascribed antiviral activities of published PIKfyve inhibitors. Apilimod, a published PIKfyve inhibitor, prevents infection by SARS-CoV-2 and other viruses. Dose-dependent inhibition of infection was observed in an infectivity assay utilizing SARS-CoV-2 strain 2019-nCoV/USA-WA1/2020. The proposed mechanism via which apilimod elicits this activity is through preventing release of viral contents from endosomes.⁷ This activity of apilimod coupled with its good tolerance as a drug when used for rheumatoid arthritis or Crohn's disease as well as a putative ability to block antiviral immune responses motivated its advancement to Phase 2 clinical trials for COVID-19 treatment.^{4–6}

We made use of a previously developed β-coronavirus assay to explore the activity of our compounds versus published PIKfyve inhibitors on β-coronavirus replication.²⁵ This assay employs a fusion of mouse hepatitis virus (MHV) with nanoLuciferase (nLuc) to yield MHV-nLuc virus. MHV belongs to the β-coronavirae genus along with SARS-CoV-2. While MHV is a common mouse pathogen, it is not infectious to humans and it has been widely used as a model to study the virulence of SARS-CoV-2.^{25,26} Furthermore, there is 94% identity between human and mouse PIKfyve. The optimal titer and time point to analyze viral replication were determined via inoculation of mouse derived-from-brain-tumor (DBT) cells by MHV-nLuc.²⁵ Accordingly, DBT cells were inoculated by MHV-nLuc with an MOI = 0.1 and luciferase measured at 10 h post-infection.

Several of the more selective compounds from Tables 1–4 and the published PIKfyve inhibitors in Figure 1 were evaluated in the optimized MHV-nLuc assay in DBT cells. All of the published inhibitors and many of our PIKfyve inhibitors, including chemical probe candidates 8 and 17, inhibited viral

Table 5. PIKfyve NanoBRET versus Viral Replication Data

compound	PIKfyve NB IC ₅₀ (nM)	PIKfyve NB pIC ₅₀	MHV replication IC ₅₀ (nM)	MHV replication pIC ₅₀	SARS-CoV-2 replication IC ₅₀ (nM)
2	2540	5.61	8470	5.07	NT ^a
5	885	6.05	485	6.31	NT
7	380	6.42	713	6.15	NT
8	11.4	7.94	71.0	7.15	73.3
10	1170	5.93	1920	5.72	NT
12	4970	5.30	5350	5.27	NT
13	1560	5.81	666	6.18	NT
14	>10 000	5.00	8050	5.09	NT
17	4.01	8.40	23.5	7.63	19.5
26	12.7	7.90	74.0	7.13	23.9
28	700	6.15	1800	5.75	NT
30	>10 000	5.00	>10 000	5.00	>10 000
apilimod	0.312	9.51	15.7	7.80	NT
YM201636	73.5	7.13	250	6.60	NT
APY0201	1.19	8.92	40.4	7.39	NT
remdesivir	NT	NT	NT	NT	86.4

^aNT: not tested.

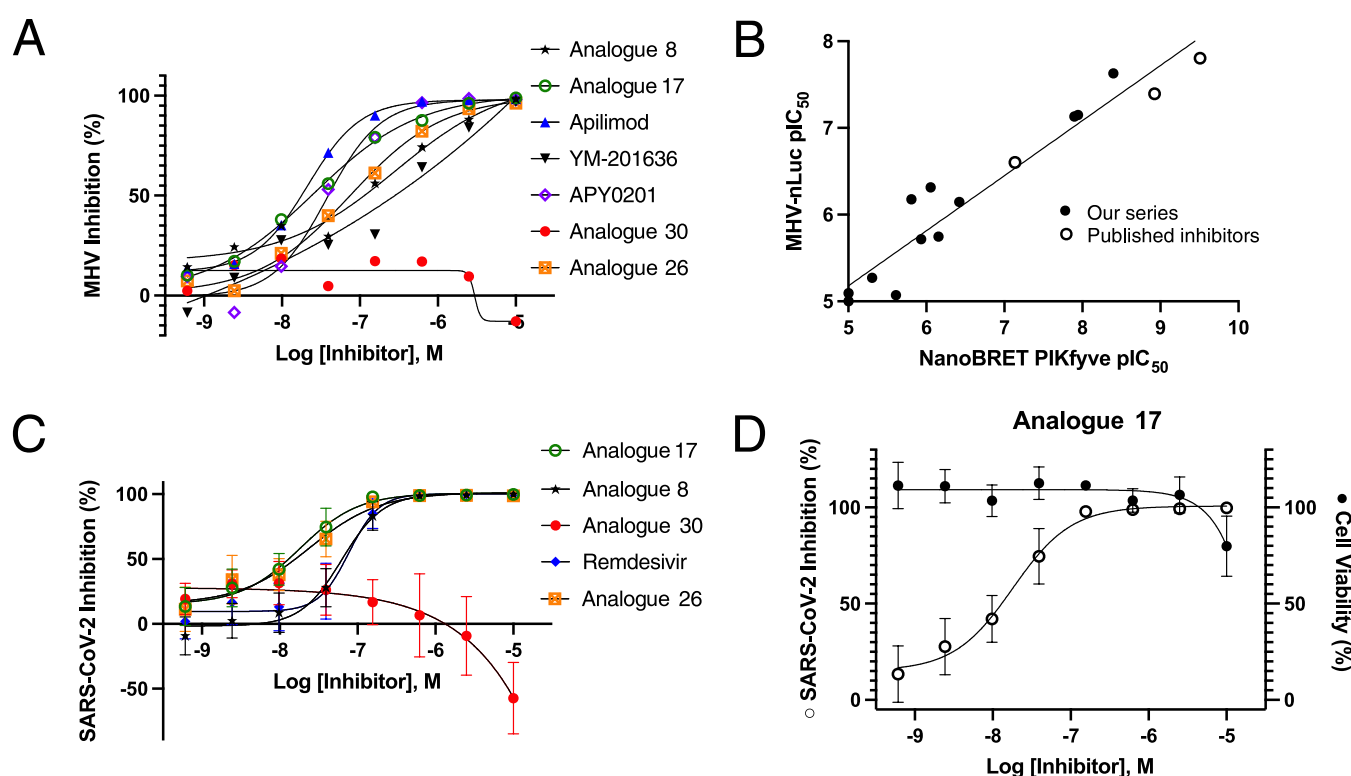


Figure 4. β -Coronavirus replication assay results. (A) Effect of PIKfyve inhibitors on replication of MHV-nLuc in DBT cells. Plot of average value for compounds that exhibit IC₅₀ < 100 nM ($n = 3$). (B) Correlation of potency for PIKfyve target engagement with inhibition of β -coronavirus replication across our series of indolyl pyrimidinamines and published PIKfyve inhibitors. The analysis uses the pIC₅₀ of the PIKfyve NanoBRET values and the pIC₅₀ of the MHV-nLuc assay values from Table 5 for every analogue tested. The linear regression drawn demonstrates an $R^2 = 0.921$. (C) Effect of PIKfyve inhibitors on viral replication in A549-ACE2 cells infected with SARS-CoV-2-nLuc ($n = 4$). Error bars represent standard error of the mean (SEM). (D) Effect of probe candidate 17 on viral replication (open circles) in A549-ACE2 cells infected with SARS-CoV-2-nLuc ($n = 4$). Cell viability determined by LDH assay (closed circles) in A549-ACE2 cells ($n = 2$). Error bars represent standard error of the mean (SEM).

replication with no significant effect on cell viability up to 10 μ M (Table 5 and Figures 4A, S3, and S4). Negative control compound 30, which lacks PIKfyve potency, failed to inhibit viral replication but was also nontoxic up to 10 μ M (Figures 4A, S3, and S4). Importantly, anti- β -coronavirus activity correlated well with potency in the PIKfyve NanoBRET assay (Table 5 and Figure 4B). The most potent PIKfyve inhibitors were also most efficacious in the antiviral assay, while those devoid of PIKfyve

inhibitory potential were unable to block viral replication. The relationship was maintained for indolyl pyrimidinamines of variable potency as well as when the published PIKfyve inhibitors from Figure 1 were added. Figure 4B shows this correlation and the linear regression fit with an $R^2 = 0.921$. That addition of these published inhibitors, with different chemotypes than our series, slightly improves the correlation ($R^2 = 0.916$ for indolyl pyrimidinamines alone) further confirms the

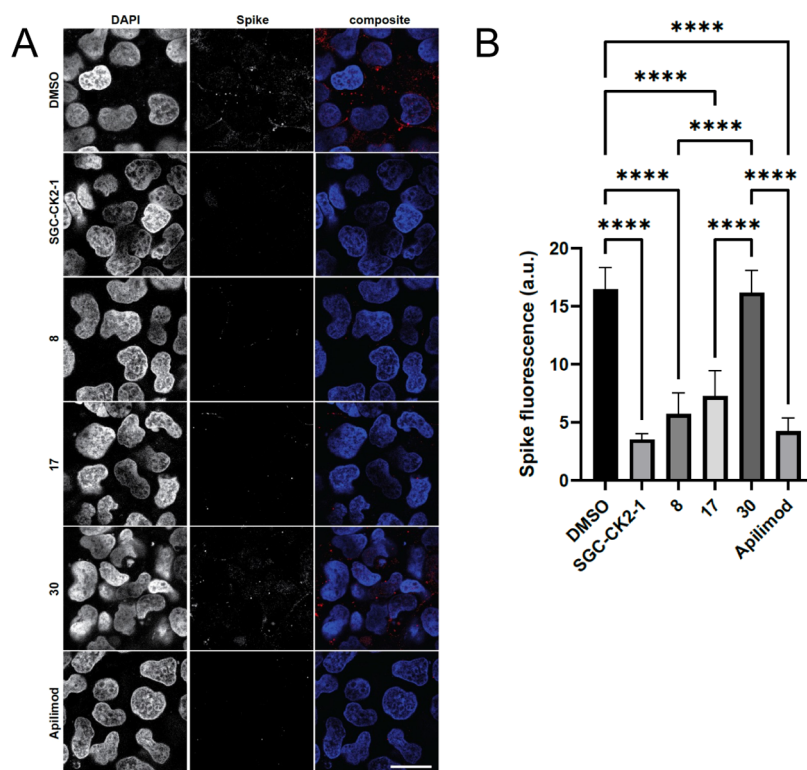


Figure 5. PIKfyve inhibitors reduce uptake of His6-SARS-CoV-2 spike protein by HEK293T-ACE2 cells. (A) Images of cells treated with 1 μ M PIKfyve inhibitors (analogues 8, 17, or apilimod), negative control (analogue 30), CK2 inhibitor (SGC-CK2-1, positive control), or DMSO (vehicle control). Cell nuclei are stained with DAPI, and the spike protein was detected using a His6 antibody. Scale bar (shown in white in the bottom right corner of the images) = 20 μ m. (B) Quantification of the His6-SARS-CoV-2 spike protein uptake. The data is from three independent experiments with $n = 6$ for each condition. AU, arbitrary units; **** p -value < 0.0001. P -values were generated using one-way analysis of variance (ANOVA) with a post-hoc Tukey's test to compare the means with one another.

relationship between PIKfyve inhibition and anti- β -coronavirus activity.

The three most efficacious inhibitors of viral replication in the MHV-nLuc assay (8, 17, and 26) and the negative control compound (30) from the indolyl pyrimidinamine series were evaluated in a SARS-CoV-2-nLuc assay in human epithelial A549-ACE2 cells (Figures 4C,D, and S5).²⁷ Remdesivir, an antiviral drug FDA-approved for use against SARS-CoV-2,²⁸ was included as a positive control compound ($IC_{50} = 86.4$ nM). Probe compound 17 was found to be the most potent inhibitor of SARS-CoV-2 replication ($IC_{50} = 19.5$ nM) and outperformed remdesivir in this assay. Analogues 8 and 26 were also potent inhibitors of SARS-CoV-2 replication with IC_{50} values that were slightly better than remdesivir (Table 5). Importantly, the PIKfyve inhibitors were generally nontoxic to the A549-ACE2 cells and only exhibited toxicity at the highest dose (Figures 4D and S5). Negative control 30 did not inhibit SARS-CoV-2 replication or elicit any toxicity.

PIKfyve Inhibitors Disrupt Multiple Mediators in the Virus Lifecycle. Since phosphatidylinositol-3-phosphate plays roles in membrane dynamics and trafficking as well as endosome processing and lysosomal function,^{29,30} PIKfyve inhibition is proposed to interrupt multiple processes that viruses hijack for entry and transmission. Reported mechanisms via which PIKfyve inhibition reduces viral infection in host cells include suppression of entry and/or through causing defective viral trafficking prior to entry, prevention of release of viral contents from endosomes, prevention of viral invasion via inhibiting host cell proteases, and/or antagonism of viral replication.^{6,7,31,32} These roles are consistent with the finding that, among other

functions, PIKfyve resides predominately in early endosomes and plays an essential role in maintaining endomembrane homeostasis.³² While engagement of the host cell receptor ACE2 is an important step in viral entry of SARS-CoV-2, subsequent entry steps can vary and be dependent on the cell type. This virus can enter host cells via both clathrin (endosomal) and nonclathrin (not reliant on endosomes) pathways.³³ The endosomal system used by SARS-CoV-2 is mediated by phosphoinositides. Endosomal PI(3,5)P₂, which is produced via the enzymatic activity of PIKfyve, is implicated as playing a particularly essential role in endosomal homeostasis and regulation of early-to-late endosome dynamics.^{34,35}

Apilimod was previously found to inhibit viral entry and replication during entry of several viruses, including SARS-CoV-2.^{32,34,35} YM201636 also prevents entry of SARS-CoV-2 S pseudovirions into HEK293/hACE2 cells, suggesting that this reduction of viral entry may be a general feature of PIKfyve inhibition.³⁵ Given these findings, we explored the impact of our PIKfyve inhibitors on viral entry. Since most human coronaviruses are endocytosed prior to infection, we hypothesized that PIKfyve inhibition could specifically impact the clathrin-mediated route of SARS-CoV-2 internalization.³⁶ Clathrin-mediated endocytosis (CME) is the primary pathway of SARS-CoV-2 cell entry.³⁷ A purified spike glycoprotein uptake assay developed by the McPherson lab enabled us to probe whether PIKfyve is required for viral entry of the SARS-CoV-2 spike protein trimer. Furthermore, since this assay relies on CME, its use probes whether this is a mechanism that is interrupted by PIKfyve inhibitors.³⁷

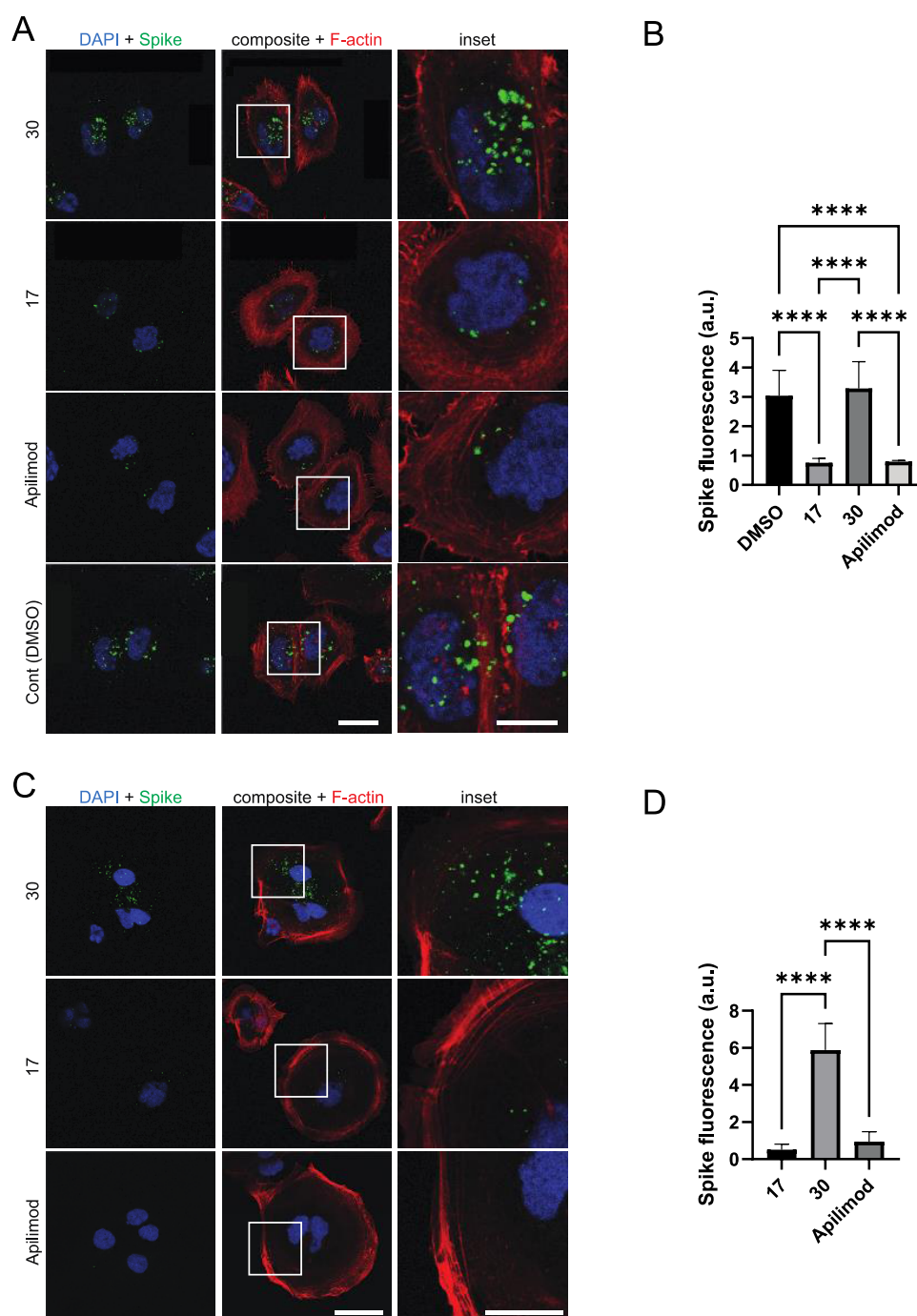


Figure 6. PIKfyve inhibitors reduce uptake of His6-SARS-CoV-2 spike protein by Calu-3 (A, B) and Caco-2 (C, D) cells. (A) Images of Calu-3 cells treated with 1 μ M PIKfyve inhibitors (analogue 17 or apilimod), PIKfyve negative control (analogue 30), or DMSO (vehicle control). Scale bar, shown in white in the bottom right corner of the images, is 20 μ m for the left and middle panels and 10 μ m for the inset. (B) Quantification of the His6-SARS-CoV-2 spike protein uptake in Calu-3 cells. (C) Images of Caco-2 cells treated with 1 μ M PIKfyve inhibitors (analogue 17 or apilimod) or PIKfyve negative control (analogue 30). Scale bar, shown in white in the bottom right corner of the images, is 40 μ m for the left and middle panels and 20 μ m for the inset. (D) Quantification of the His6-SARS-CoV-2 spike protein uptake in Caco-2 cells. The data is from three independent experiments for each cell line with $n = 6$ for each condition. AU, arbitrary units; **** p -value < 0.0001. For panels (A) and (C), cell nuclei are stained with DAPI, F-actin stained with phalloidin to define cell boundaries, and spike protein detected using a His6 antibody. For panels (B) and (D), p -values were generated using one-way ANOVA, with a post-hoc Tukey's test to compare the means with one another.

His6-tagged spike protein was incubated with and internalized by HEK293T-ACE2 cells in the presence of either dimethyl sulfoxide (DMSO) (vehicle control), 1 μ M SGC-CK2-1 (positive control), or 1 μ M PIKfyve inhibitor (Figure 5). When intercellular spike protein was visualized and quantified, vehicle-treated cells showed efficient uptake of the His6-tagged

spike protein. In accordance with previous studies, treatment of the cells with 1 μ M SGC-CK2-1 efficiently decreased spike protein uptake.²⁵ Similarly, treatment of the cells with 1 μ M PIKfyve inhibitors from our series (8 and 17) or apilimod also significantly reduced spike protein uptake versus the vehicle-treated control cells. Notably, 1 μ M negative control analogue

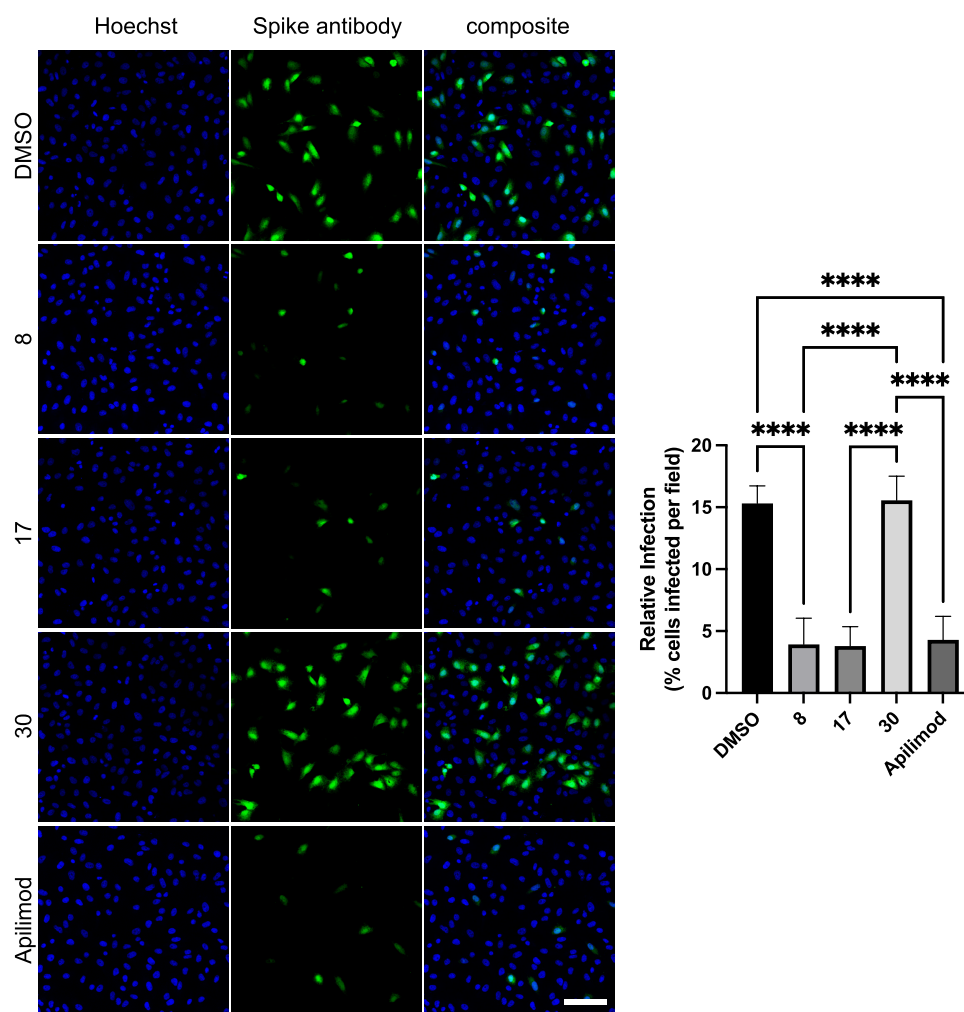


Figure 7. Uptake of lentivirus pseudotyped with the SARS-CoV-2 spike glycoprotein is inhibited by PIKfyve inhibitors. Calu-3 cells were incubated with 1 μ M of compound (or DMSO) for 1 h followed by the addition of the lentivirus pseudotyped with the SARS-CoV-2 spike glycoprotein for 12 h. Cells were fixed and stained with Hoechst to label the nuclei. Cells were also imaged for spike expression using spike antibody and visualized via Alexa Fluor 488, following transduction of the pseudovirus. Scale bars (shown in white in the bottom right corner of the images) = 100 μ m. Bar graph shows the quantification of SARS-CoV-2 pseudovirus infection from experiments: $n = 9$ from three independent experiments, mean \pm standard deviation (SD); one-way ANOVA followed Tukey's test. **** $p < 0.0001$.

30 demonstrated no effect on spike protein uptake in HEK293T-ACE2 cells. Next, since high levels of surface protease expression can promote an alternative route of viral entry via membrane fusion, the uptake of His6-tagged spike protein in Calu-3 and Caco-2 cells was imaged and quantified (Figure 6).³⁸ These more physiologically relevant cell lines were chosen for their high ACE2 expression (Calu-3 and Caco-2) and high transmembrane serine protease (TMPRSS2) expression (Calu-3 only).^{39,40} As we observed in HEK293T-ACE2 cells, PIKfyve inhibitors (analogue 17 or apilimod) efficiently reduced spike protein uptake versus cells treated with DMSO and/or negative control analogue 30. In both cell lines, PIKfyve inhibitors produced >75% decrease in spike protein uptake, with the most robust reduction (>91%) observed in Caco-2 cells. The fact that uptake was significantly reduced in different cell lines despite their variable expression levels of TMPRSS2 supports that endocytosis is the primary pathway for SARS-CoV-2 uptake into cells. Our chemical series of PIKfyve inhibitors effectively prevents CME-mediated cell entry of the SARS-CoV-2 spike protein.

To confirm that the inhibition of CME observed for the SARS-CoV-2 spike protein was also observed for the corresponding pseudovirus, we explored uptake of the lentivirus pseudotyped with SARS-CoV-2 spike glycoprotein by Calu-3 cells. We observed inhibition of pseudoviral entry versus DMSO-treated cells when cells were treated with PIKfyve inhibitors, including analogues 8 and 17 as well as apilimod. Treatment of cells with negative control compound 30 did not inhibit pseudoviral entry (Figure 7). In parallel, bald lentivirus containing the eGFP gene was introduced to Calu-3 cells. This lentiviral pseudovirion was selected as a negative control for studying the viral entry mediated by CME. When treated with the same compounds (apilimod and analogues 8, 17, and 30) or DMSO, entry of bald lentivirus was not impacted (Figure S6). Our PIKfyve inhibitors do not affect viral entry in general. Rather, since PIKfyve inhibitors reduced entry of lentivirus pseudotyped with SARS-CoV-2 spike glycoprotein but not entry of bald lentivirus, the effect of our compounds is specific to viral particles being internalized via the spike protein interacting with ACE2 receptors, a process that utilizes CME.

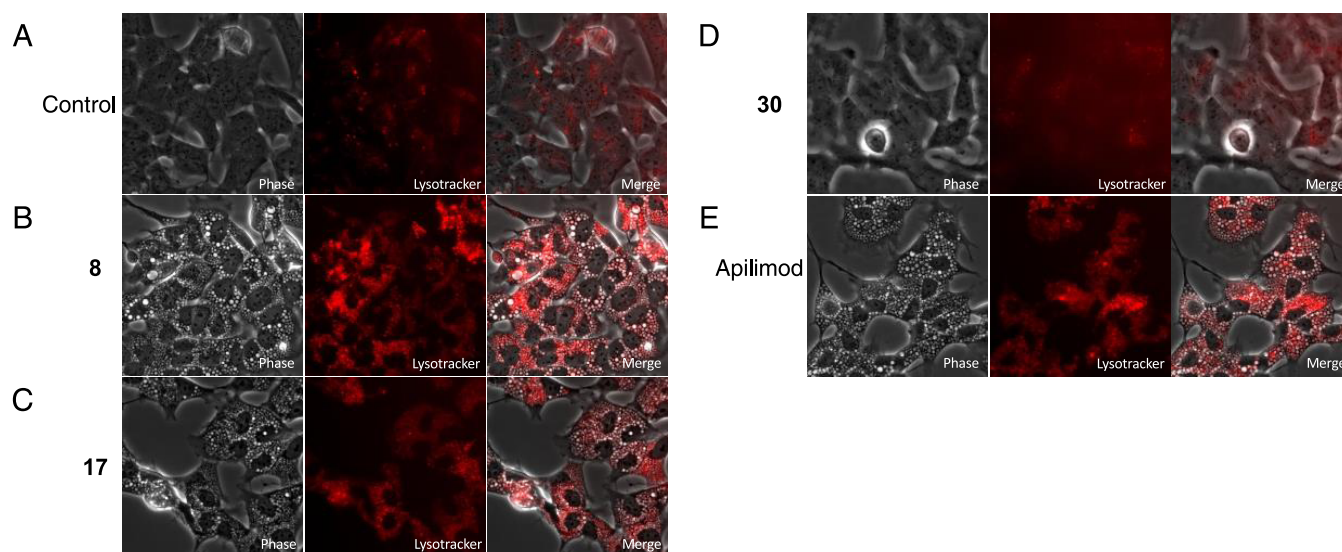
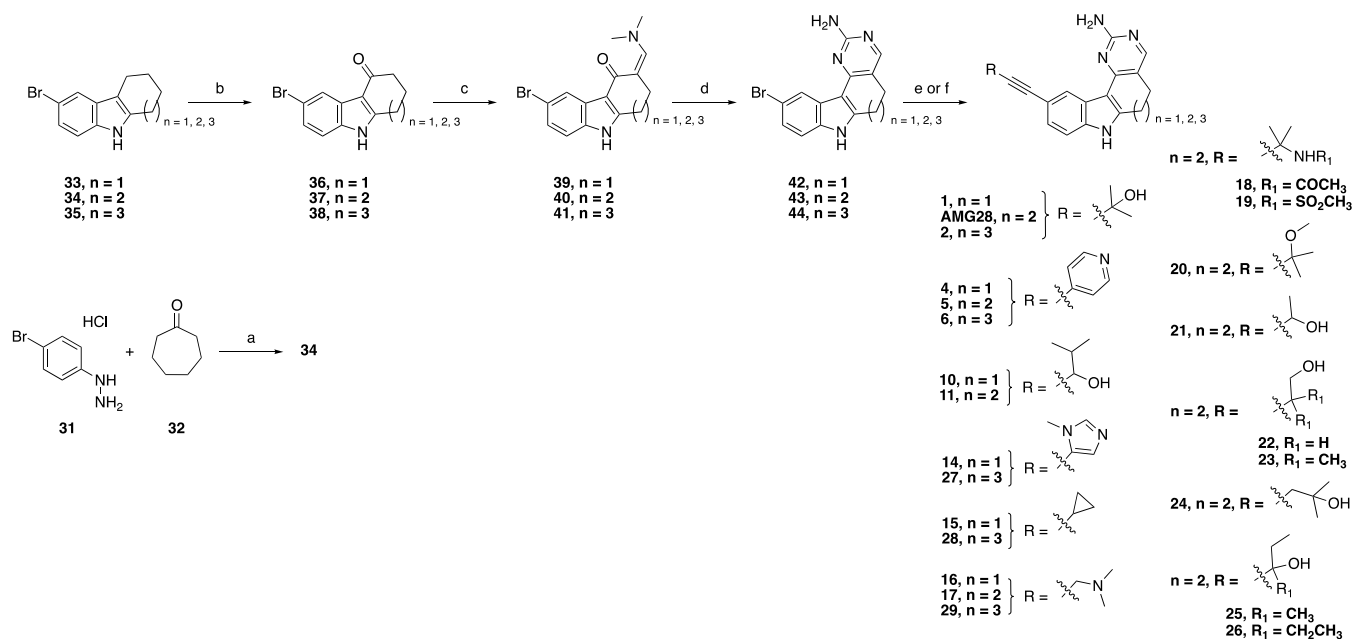


Figure 8. PIKfyve inhibitors impact lysosomal homeostasis. Panels (A–E) show that 50 nM LysoTracker was added 24 h after treatment with 0.05% DMSO (A), 5 μ M 8 (B), 5 μ M 17 (C), 5 μ M 30 (D), or 5 μ M apilimod (E) and imaged at 40 \times .

Scheme 1. Synthesis of Analogues 1, 2, 4–6, 10–11, 14–29, and AMG28^a



^aReagents and conditions: (a) AcOH, 50–120 $^{\circ}\text{C}$, 3 h, 70%; (b) DDQ, tetrahydrofuran (THF)/water, 0 $^{\circ}\text{C}$, 45 min, 53–87%; (c) Bredereck's reagent, toluene, or neat, 110 $^{\circ}\text{C}$, 3–12 h; (d) NaOMe, guanidine hydrochloride, *i*PrOH, 100 $^{\circ}\text{C}$, 12 h, 12–38% over two steps; (e) For 1, 2, 4–6, 10, 11, 14–17, 27–29, and AMG28: Alkyne R, triethylamine (TEA) or *N,N*-diisopropylamine (DIPA), Pd(PPh₃)₄, CuI, *N,N*-dimethylformamide (DMF), or *N,N*-dimethylacetamide (DMA), 100 $^{\circ}\text{C}$, 12 h, 1.5–22%; (f) For 18–26: Alkyne R, DIPA, PdCl₂(PPh₃)₂, CuI, propanol, 100 $^{\circ}\text{C}$, 12 h, 2.4–15%.

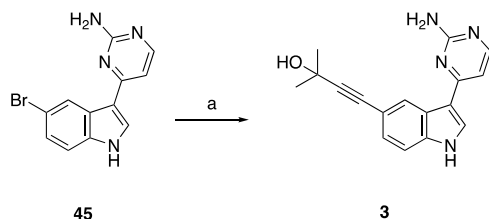
Studies in multiple cell types have demonstrated that the PI(3,5)P₂ depletion following PIKfyve inhibition or deletion leads to significant swelling of endolysosomes.^{3,41–43} Using apilimod as a tool, inhibition of PIKfyve was linked with disruption of lysosomal function and endolysosomal swelling (vacuolization). The shape and size of endosomes and lysosomes were altered due to apilimod treatment. This activity contributes to the cytotoxicity exerted by apilimod in B-NHL.² Most viruses, including hepatitis C, dengue, and West Nile, exit cells via the biosynthetic secretory pathway and transmit throughout the body.^{44,45} However, it was recently reported

that β -coronaviruses hijack lysosomes to exit cells and spread systemically. To be able to exist in and exit via lysosomes of infected cells, SARS-CoV-2 deacidify lysosomes and weaken their ability to destroy the virus.⁴⁶ Thus, targeting lysosomes has been suggested as a method to stop transmission of these viruses. To probe whether our series also disrupts lysosomal homeostasis, we treated SH-SY5Y neuroblastoma cells with DMSO or 5 μ M analogues 8, 17, 30, or apilimod for 24 h, stained with LysoTracker, and imaged them. Fluorescence in these images was also quantified (Figure S7). As shown in Figure 8A–E, vacuoles are present in cells treated with 8, 17, or apilimod, but

not in those treated with DMSO or **30**. Furthermore, there is overlap between the localization of LysoTracker stain and vacuoles in Figure 8B,C,E, which is consistent with most of them being lysosomes. Induced lysosomal dysfunction by PIKfyve inhibitors is a potential mechanism that could be used to slow the spread of β -coronaviruses like SARS-CoV-2.

Chemistry. Similar routes were employed to prepare all intermediates and final compounds. Preparation of AMG28 began with Fischer indole synthesis to produce **34**. Indole **34** was also used to prepare analogues **5**, **8**, **11**, **13**, and **17–26**. Synthesis of analogues **1**, **4**, **7**, **10**, **12**, and **14–16** commenced with commercially available indole **33**, while commercially available indole **35** was used to prepare analogues **2**, **6**, **9**, and **27–30**. Intermediates **36–38** were obtained from indoles **33–35** via selective oxidation with 2,3-dichloro-5,6-dicyano-1,4-benzoquinone (DDQ). Next, intermediates **39–41** were prepared from **36–38** by refluxing with Brederick's reagent and then cyclized to the corresponding aminopyrimidines **42–44** via reacting with a guanidinium species. Final PIKfyve inhibitors **1**, **2**, **4–6**, **10–11**, **14–29**, and AMG28 were synthesized from **42–44** under Sonogashira coupling conditions (Scheme 1). Similarly, final compound **3** was obtained using commercially available indole **45** and Sonogashira coupling conditions (Scheme 2). Finally, aminopyrimidines **42–44** were used to access PIKfyve inhibitors **7–9**, **12**, **13**, and **30** via the Suzuki cross-coupling methodology (Scheme 3).

Scheme 2. Synthesis of Analogue 3^a



^aReagents and conditions: (a) 2-methylbut-3-yn-2-ol, TEA, Pd(PPh₃)₄, CuI, DMA, 100 °C, 12 h, 4.4%.

CONCLUSIONS

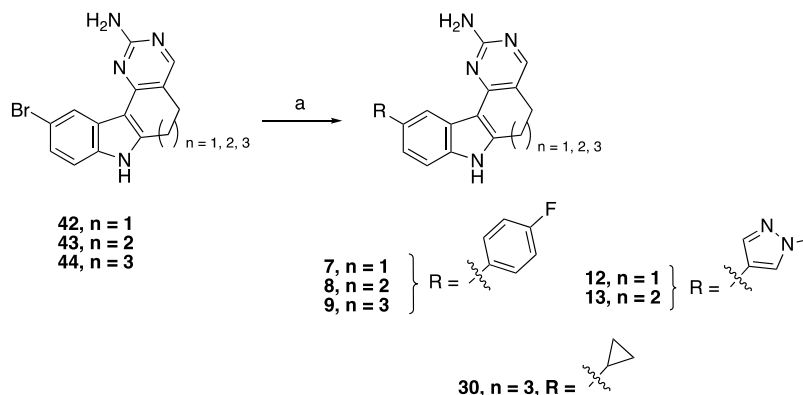
We suggest analogue **17** as the optimal PIKfyve chemical probe from our indolyl pyrimidinamine series. Analogue **17** meets SGC probe criteria²³ based on its potency in the PIKfyve

enzymatic (IC₅₀ < 100 nM) and NanoBRET assays (IC₅₀ < 1 μ M) and selectivity across the kinome (S₁₀(1 μ M) = 0.02), with only two kinases (MAP4K5 and MYLK4) inhibited within 30-fold of its activity in the PIKfyve enzymatic assay. Furthermore, analogue **30** is a suitable negative control to be distributed and utilized alongside the PIKfyve chemical probe due to its >100 \times lower potency in the PIKfyve enzymatic and NanoBRET assays coupled with its narrow kinome-wide selectivity (S₁₀(1 μ M) = 0). Multiple PIKfyve active inhibitors from our series potently inhibited β -coronavirus replication in MHV-NLuc reporter and SARS-CoV-2-nLuc assays. A deeper dive into the mechanisms via which PIKfyve inhibition disrupts the viral lifecycle demonstrated that analogues **8** and **17** impact both viral entry, specifically mediated by CME, and a potential route of systemic viral spread. In comparing our data with that generated using published PIKfyve inhibitors, we provide an orthogonal scaffold capable of PIKfyve inhibition in cells as a chemical probe set (positive and negative control) to be used by the scientific community to interrogate PIKfyve biology in cells.

EXPERIMENTAL SECTION

Chemistry: General Information. Reagents were obtained from verified commercial suppliers and used without further characterization or purification. Temperatures are reported in degree celsius (°C); the solvent was removed via a rotary evaporator under reduced pressure; and thin layer chromatography was used to monitor the progress of reactions that were executed under a blanket of nitrogen unless otherwise noted. The following abbreviations are used in schemes and/or experimental procedures: mmol (millimoles), μ mol (micromoles), mg (milligrams), min (minutes), equiv (equivalent(s)), r.t. (room temperature), sec (seconds), and h (hours). ¹H NMR and/or additional microanalytical data was collected for intermediates and final compounds to confirm their identity and assess their purity. ¹H and ¹³C NMR spectra were obtained in DMSO-*d*₆, CDCl₃, or CD₃OD-*d*₄ and recorded using Varian or Bruker spectrometers. Magnet strength is indicated in each corresponding line listing. Peak positions are listed in parts per million (ppm) and calibrated versus the shift of the indicated deuterated solvent; coupling constants (*J* values) are reported in hertz (Hz); and multiplicities are included as follows: singlet (s), doublet (d), doublet of doublets/triplets/quartets (dd/dt/dq), triplet (t), triplet of doublets/triplets (td/tt), quartet (q), quartet of doublets (qd), pentent (p), and multiplet (m). Purity was determined using high-performance liquid chromatography (HPLC). The synthesis of final products was performed by ChemSpace LLC. Identity and purity of these compounds was confirmed upon receipt via NMR and additional microanalytical methods. All final compounds are >95% pure

Scheme 3. Synthesis of Analogues 7–9, 12, 13, and 30^a



^aReagents and conditions: (a) Boronic acid R, K₂CO₃, or K₃PO₄, Pd(PPh₃)₄, or Pd(dppf)Cl₂, dioxane, and/or water, 80–95 °C, 12 h, 4.0–44%.

by HPLC analysis. Confirmatory HPLC traces are included in the Supporting Information.

2-Bromo-5,6,7,8,9,10-hexahydrocyclohepta[b]indole (34). A suspension of **31** (2.0 g, 10.7 mmol) in AcOH (10 mL) was heated at 50 °C for 30 min, then **32** (2.4 g, 21.4 mmol) was added in one portion and the reaction mixture was refluxed for 3 h. After cooling to r.t., AcOH was removed under reduced pressure and the residue was dissolved in EtOAc. The organic phase was washed with water and brine, dried over anhydrous Na₂SO₄, and concentrated *in vacuo*. The residue was purified with column chromatography (SiO₂, 0–40% EtOAc in hexane) to yield **34** (1.14 g, 40% yield). ¹H NMR (400 MHz, CDCl₃) δ 7.68 (s, 1H), 7.59 (d, *J* = 1.9 Hz, 1H), 7.17 (dd, *J* = 8.5, 1.9 Hz, 1H), 7.10 (d, *J* = 8.5 Hz, 1H), 2.84–2.79 (m, 2H), 2.78–2.73 (m, 2H), 1.93–1.86 (m, 2H), 1.81–1.71 (m, 4H). ¹³C NMR (101 MHz, CDCl₃) δ 139.04, 132.95, 131.20, 123.37, 120.47, 113.70, 112.45, 111.69, 31.79, 29.68, 28.70, 27.49, 24.71. HPLC purity: >95%. HRMS calculated for C₁₃H₁₅BrN [M + H]⁺: 264.0388. Found: 264.0382.

General Procedure for the Synthesis of Compounds 36–38:

Procedure A. A solution of **33–35** (1 equiv) in THF (0.1 M) and H₂O (1.0 M) was cooled to 0 °C and treated with a solution of DDQ (2 equiv) in THF (0.5 M) at such a rate that the reaction mixture did not exceed 4 °C. The resulting solution was allowed to stir for an additional 45 min at 0 °C. The solution was concentrated to dryness under reduced pressure. The resulting solids were suspended in EtOAc and saturated NaHCO₃ solution. The solids were collected by filtration and washed with additional saturated NaHCO₃ solution, followed by water and dried *in vacuo* to give the title compounds that were used in the next step without further purification.

6-Bromo-1,2,3,9-tetrahydro-4H-carbazol-4-one (36). The reaction was carried out according to general procedure A using **33** (8.05 g, 32.1 mmol) in THF (300 mL) and water (35 mL) and DDQ (14.6 g, 64.3 mmol) in THF (130 mL) to afford the title compound (7.45 g, 87% yield). ¹H NMR (400 MHz, DMSO-*d*₆) δ 12.07 (s, 1H), 8.05 (d, *J* = 1.9 Hz, 1H), 7.37 (d, *J* = 8.5 Hz, 1H), 7.29 (dd, *J* = 8.5, 2.0 Hz, 1H), 2.96 (t, *J* = 6.2 Hz, 2H), 2.43 (dd, *J* = 7.1, 5.6 Hz, 2H), 2.11 (p, *J* = 6.3 Hz, 2H). ¹³C NMR (101 MHz, DMSO-*d*₆) δ 192.92, 153.51, 134.66, 126.23, 124.91, 122.19, 114.13, 113.61, 111.23, 37.61, 23.24, 22.65. HPLC purity: >95%. HRMS calculated for C₁₂H₁₁BrNO [M + H]⁺: 264.0024. Found: 264.0018.

2-Bromo-6,7,8,9-tetrahydrocyclohepta[b]indol-10(5H)-one (37). The reaction was carried out according to general procedure A using **34** (16.5 g, 62.6 mmol) in THF (500 mL) and water (70 mL) and DDQ (28.4 g, 125 mmol) in THF (250 mL) to afford the title compound (14.0 g, 80% yield). ¹H NMR (400 MHz, DMSO-*d*₆) δ 8.28 (d, *J* = 2.0 Hz, 1H), 7.32 (d, *J* = 8.5 Hz, 1H), 7.26 (dd, *J* = 8.5, 2.0 Hz, 1H), 3.15–3.08 (m, 2H), 2.70–2.63 (m, 2H), 1.97–1.89 (m, 2H), 1.87–1.80 (m, 2H). ¹³C NMR (101 MHz, DMSO-*d*₆) δ 196.50, 150.30, 133.90, 129.11, 124.68, 123.01, 114.04, 113.26, 113.03, 42.72, 27.21, 24.21, 21.80. HPLC purity: >95%. HRMS calculated for C₁₃H₁₃BrNO [M + H]⁺: 278.0181. Found: 278.0174.

2-Bromo-5,6,7,8,9,10-hexahydro-11H-cycloocta[b]indol-11-one (38). The reaction was carried out according to general procedure A using **35** (10.5 g, 37.6 mmol) in THF (300 mL) and water (35 mL) and DDQ (17.1 g, 75.3 mmol) in THF (150 mL) to afford the title compound (6.43 g, 53% yield). ¹H NMR (400 MHz, DMSO-*d*₆) δ 8.40–8.34 (m, 1H), 7.35 (dd, *J* = 8.5, 0.6 Hz, 1H), 7.27 (dd, *J* = 8.5, 2.0 Hz, 1H), 3.27 (t, *J* = 7.1 Hz, 2H), 2.82 (t, *J* = 7.2 Hz, 2H), 1.75–1.70 (m, 4H), 1.41–1.37 (m, 2H). ¹³C NMR (101 MHz, DMSO-*d*₆) δ 195.60, 147.78, 133.38, 128.81, 124.54, 123.19, 115.47, 114.24, 113.22, 41.02, 26.84, 24.55, 23.34, 22.89. HPLC purity: >95%. HRMS calculated for C₁₄H₁₅BrNO [M + H]⁺: 292.0337. Found: 292.0330.

General Procedure for the Synthesis of Compounds 39–41:

Procedure B. To a suspension of **36–38** (1 equiv) in toluene (0.3 M, unless otherwise noted) was added Bredereck's reagent (3 equiv). The resulting mixture was refluxed either for 3 h or overnight. After cooling to r.t., toluene was decanted (unless otherwise noted) and the viscous residue was dried *in vacuo* to give the crude title compounds that were used in the next step without further purification.

(Z)-6-Bromo-3-((dimethylamino)methylene)-1,2,3,9-tetrahydro-4H-carbazol-4-one (39). The reaction was carried out according to

general procedure B using **36** (7.44 g, 28.2 mmol) in toluene (100 mL) and Bredereck's reagent (14.7 g, 84.6 mmol) at 110 °C overnight to afford the crude title compound (7.10 g, 74% yield).

(Z)-2-Bromo-9-((dimethylamino)methylene)-6,7,8,9-tetrahydrocyclohepta[b]indol-10(5H)-one (40). The reaction was carried out according to general procedure B using **37** (14.0 g, 62.6 mmol) in toluene (200 mL) and Bredereck's reagent (28.4 g, 126 mmol) at 110 °C overnight to afford the crude title compound (13.0 g, 77% yield).

(Z)-2-Bromo-10-((dimethylamino)methylene)-5,6,7,8,9,10-hexahydro-11H-cycloocta[b]indol-11-one (41). The reaction was carried out according to general procedure B using **38** (6.39 g, 21.9 mmol) and Bredereck's reagent (7.63 g, 43.8 mmol) at 110 °C for 3 h to afford the crude title compound (5.56 g, 75% yield) after trituration with *n*-hexane and methyl *tert*-butyl ether (MTBE), filtration, and drying *in vacuo*.

General Procedure for the Synthesis of Compounds 42–44:

Procedure C. Guanidine hydrochloride (1.5–2 equiv) was added to a hot freshly prepared solution of NaOMe (1.5–3 equiv of Na in 0.4 M methanol), and the mixture was stirred for 10 min, diluted with isopropyl alcohol (IPA, 0.2 M), and filtered. **39–41** (1 equiv) were added to the filtrate, and the mixture was stirred at 100 °C overnight. After completion of the reaction, the mixture was cooled to r.t. and concentrated. The residue was diluted with water and extracted with EtOAc. The organic layer was washed with water, brine, dried over Na₂SO₄, and evaporated under reduced pressure. The crude residue was purified either by flash column chromatography on SiO₂ with 0–10% MeOH in CH₂Cl₂ (**42**, **43**) or filtered under vacuum with water (**44**) to obtain the title compounds.

10-Bromo-6,7-dihydro-5H-pyrimido[5,4-*c*]carbazol-2-amine (42). The reaction was carried out according to general procedure C using NaOMe (1.53 g, 66.6 mmol of Na in 50 mL MeOH), guanidine hydrochloride (3.18 g, 33.3 mmol), IPA (100 mL), and **39** (7.08 g, 22.2 mmol) at 110 °C overnight to afford the title compound (1.10 g, 16% yield). ¹H NMR (400 MHz, DMSO-*d*₆) δ 11.84 (s, 1H), 8.39 (d, *J* = 2.0 Hz, 1H), 7.35 (d, *J* = 8.5 Hz, 1H), 7.24 (dd, *J* = 8.5, 2.1 Hz, 1H), 6.26 (s, 2H), 2.99 (t, *J* = 7.5 Hz, 2H), 2.84 (t, *J* = 7.7 Hz, 2H). ¹³C NMR (101 MHz, DMSO-*d*₆) δ 162.54, 159.75, 153.58, 145.82, 135.18, 126.21, 123.93, 122.70, 113.42, 113.10, 112.95, 108.41, 23.46, 21.56. HPLC purity: >95%. HRMS calculated for C₁₄H₁₂BrN₄ [M + H]⁺: 315.0245. Found: 315.0239.

11-Bromo-5,6,7,8-tetrahydropyrimido[4',5':3,4]cyclohepta[1,2-*b*]indol-2-amine (43). The reaction was carried out according to general procedure C using NaOMe (3.57 g, 77.8 mmol of Na in 100 mL MeOH), guanidine hydrochloride (7.43 g, 77.8 mmol), IPA (200 mL), and **40** (13.0 g, 38.9 mmol) at 110 °C overnight to afford the title compound (4.70 g, 39% yield). ¹H NMR (400 MHz, CD₃OD-*d*₄) δ 8.81 (dd, *J* = 1.9, 0.6 Hz, 1H), 7.84 (s, 1H), 7.21 (dd, *J* = 8.5, 1.9 Hz, 1H), 7.17 (dd, *J* = 8.5, 0.7 Hz, 1H), 3.16 (t, *J* = 6.7 Hz, 2H), 2.70–2.62 (m, 2H), 2.06–1.97 (m, 2H). ¹³C NMR (101 MHz, CD₃OD-*d*₄) δ 164.10, 163.01, 156.66, 146.06, 136.50, 130.73, 126.47, 125.86, 122.82, 114.66, 112.74, 111.55, 31.23, 30.72, 25.49. HPLC purity: >95%. HRMS calculated for C₁₅H₁₄BrN₄ [M + H]⁺: 329.0402. Found: 329.0395.

12-Bromo-6,7,8,9-tetrahydro-5H-pyrimido[4',5':3,4]cycloocta[1,2-*b*]indol-2-amine (44). The reaction was carried out according to general procedure C using NaOMe (1.10 g, 24.0 mmol of Na in 50 mL MeOH), guanidine hydrochloride (2.30 g, 24.0 mmol), IPA (100 mL), and **41** (5.50 g, 16.0 mmol) at 110 °C overnight to afford the title compound (2.80 g, 51% yield). ¹H NMR (400 MHz, DMSO-*d*₆) δ 11.38 (s, 1H), 7.99 (s, 1H), 7.92 (d, *J* = 1.9 Hz, 1H), 7.18 (d, *J* = 8.5 Hz, 1H), 7.10 (dd, *J* = 8.5, 2.0 Hz, 1H), 6.33 (s, 1H), 2.96–2.86 (m, 2H), 2.47–2.37 (m, 2H), 1.72–1.57 (m, 4H). ¹³C NMR (101 MHz, DMSO-*d*₆) δ 162.06, 161.89, 157.82, 142.25, 142.09, 134.27, 134.12, 129.60, 129.56, 123.63, 122.44, 119.62, 112.26, 112.21, 112.00, 108.83, 108.80, 30.76, 27.58, 27.52, 26.65, 20.67. HPLC purity: >95%. HRMS calculated for C₁₆H₁₆BrN₄ [M + H]⁺: 343.0558. Found: 343.0553.

General Procedure for the Synthesis of Compounds 1–6, 10, 11, 14–17, 27–29, and AMG28: Procedure D. A mixture of **42–45** (1 equiv), alkyne (1.5–5 equiv), and TEA or DIPA (1–3 equiv) in DMF or DMA (0.2–0.8 M) was degassed, followed by addition of

Pd(PPh₃)₄ (0.05–0.1 equiv) and CuI (0.05–0.2 equiv). The reaction mixture was heated to 100 °C and stirred overnight. After completion of the reaction, the mixture was cooled to r.t., diluted with EtOAc, and passed through a thin pad of celite. The filtrate was concentrated *in vacuo* and the crude residue was purified by preparative HPLC (10–100% MeOH in H₂O + 0.1% TFA) to give the title compounds.

4-(2-Amino-6,7-dihydro-5H-pyrimido[5,4-c]carbazol-10-yl)-2-methylbut-3-yn-2-ol (1). The reaction was carried out according to general procedure D using **42** (148 mg, 0.47 mmol), 2-methylbut-3-yn-2-ol (79 mg, 0.94 mmol), TEA (95 mg, 0.94 mmol), Pd(PPh₃)₄ (55 mg, 47 μmol), and CuI (18 mg, 94 μmol) in DMF (1.5 mL) at 100 °C overnight to afford the title compound (28 mg, 19% yield). ¹H NMR (500 MHz, DMSO-*d*₆) δ 11.79 (s, 1H), 8.28 (d, *J* = 1.6 Hz, 1H), 7.92 (d, *J* = 4.1 Hz, 1H), 7.35 (d, *J* = 8.3 Hz, 1H), 7.12 (dd, *J* = 8.4, 1.7 Hz, 1H), 6.20 (s, 2H), 5.40 (s, 1H), 2.97 (t, *J* = 7.8 Hz, 2H), 2.83 (t, *J* = 7.8 Hz, 2H), 1.50 (s, 6H). ¹³C NMR (126 MHz, DMSO-*d*₆) δ 162.74, 159.85, 153.80, 145.41, 135.85, 124.88, 124.35, 123.77, 114.35, 113.05, 111.69, 108.79, 93.53, 82.01, 63.66, 31.88, 23.56, 21.58. HPLC purity: 95.03%. HRMS (ESI): *m/z* calculated for C₁₉H₁₉N₄O [M + H]⁺: 319.1559. Found: 319.1555.

4-(2-Amino-5,6,7,8-tetrahydropyrimido[4',5':3,4]cyclohepta[1,2-*b*]indol-11-yl)-2-methylbut-3-yn-2-ol (AMG28). The reaction was carried out according to general procedure D using **43** (198 mg, 0.60 mmol), 2-methylbut-3-yn-2-ol (101 mg, 1.2 mmol), TEA (122 mg, 1.2 mmol), Pd(PPh₃)₄ (70 mg, 60 μmol), and CuI (18 mg, 60 μmol) in DMF (1.5 mL) at 100 °C overnight to afford the title compound (3.2 mg, 1.6% yield). The analytical data for AMG28 matches that previously reported.⁴⁷ ¹H NMR (850 MHz, CD₃OD-*d*₄) δ 8.74 (s, 1H), 7.88 (s, 1H), 7.26 (d, *J* = 8.3 Hz, 1H), 7.23–7.17 (m, 1H), 3.23 (t, *J* = 6.6 Hz, 2H), 2.76–2.70 (m, 2H), 2.12–2.05 (m, 2H), 1.59 (s, 6H). HPLC purity: 96.35%.

4-(2-Amino-6,7,8,9-tetrahydro-5H-pyrimido[4',5':3,4]cycloocta[1,2-*b*]indol-12-yl)-2-methylbut-3-yn-2-ol (2). The reaction was carried out according to general procedure D using **44** (198 mg, 0.57 mmol), 2-methylbut-3-yn-2-ol (73 mg, 0.87 mmol), TEA (117 mg, 1.16 mmol), Pd(PPh₃)₄ (33 mg, 30 μmol), and CuI (6.0 mg, 30 μmol) in DMA (1.0 mL) at 100 °C overnight to afford the title compound (13.2 mg, 6.6% yield). ¹H NMR (850 MHz, CD₃OD-*d*₄) δ 8.08 (s, 1H), 7.87 (d, *J* = 1.5 Hz, 1H), 7.24 (dd, *J* = 8.3, 0.7 Hz, 1H), 7.15 (dd, *J* = 8.3, 1.6 Hz, 1H), 3.06–2.99 (m, 2H), 2.64–2.59 (m, 2H), 1.86–1.79 (m, 4H), 1.56 (s, 6H). ¹³C NMR (214 MHz, CD₃OD-*d*₄) δ 165.02, 163.06, 159.12, 143.29, 137.11, 135.87, 135.82, 131.42, 131.36, 129.08, 126.40, 124.54, 115.64, 111.45, 110.34, 92.31, 84.41, 66.02, 32.26, 31.96, 28.97, 28.23. HPLC purity: 95.56%. HRMS (ESI): *m/z* calculated for C₂₁H₂₃N₄O [M + H]⁺: 347.1872. Found: 347.1868.

4-(3-(2-Aminopyrimidin-4-yl)-1H-indol-5-yl)-2-methylbut-3-yn-2-ol (3). The reaction was carried out according to general procedure D using **45** (396 mg, 1.37 mmol), 2-methylbut-3-yn-2-ol (345 mg, 4.11 mmol), TEA (277 mg, 2.74 mmol), Pd(PPh₃)₄ (159 mg, 0.14 mmol), and CuI (19 mg, 0.14 mmol) in DMA (3.0 mL) at 100 °C overnight to afford the title compound (17.7 mg, 4.4% yield). The analytical data for **3** matches that previously reported.²¹ ¹H NMR (400 MHz, CD₃OD-*d*₄) δ 8.59 (s, 1H), 8.17 (s, 2H), 8.07 (d, *J* = 5.8 Hz, 1H), 7.41 (d, *J* = 8.3 Hz, 1H), 7.27 (d, *J* = 8.7 Hz, 1H), 7.12 (d, *J* = 6.0 Hz, 1H), 1.60 (s, 6H). HPLC purity: 100%. HRMS (ESI): *m/z* calculated for C₁₇H₁₆N₄O [M + H]⁺: 293.1402. Found: 293.1397.

10-(Pyridin-4-ylethynyl)-6,7-dihydro-5H-pyrimido[5,4-*c*]carbazol-2-amine (4). The reaction was carried out according to general procedure D using **42** (140 mg, 0.44 mmol), 4-ethynylpyridine (92 mg, 0.88 mmol), TEA (90 mg, 0.88 mmol), Pd(PPh₃)₄ (52 mg, 44 μmol), and CuI (17 mg, 88 μmol) in DMF (1.5 mL) at 100 °C overnight to afford the title compound (33 mg, 22% yield). ¹H NMR (500 MHz, DMSO-*d*₆) δ 11.93 (s, 1H), 8.63 (d, *J* = 5.1 Hz, 2H), 8.52 (s, 1H), 7.94 (s, 1H), 7.54–7.49 (m, 2H), 7.46 (d, *J* = 8.3 Hz, 1H), 7.35 (dd, *J* = 8.3, 1.7 Hz, 1H), 6.24 (s, 2H), 3.00 (t, *J* = 7.8 Hz, 2H), 2.86 (t, *J* = 7.8 Hz, 2H). ¹³C NMR (126 MHz, DMSO-*d*₆) δ 162.73, 159.63, 153.94, 149.90, 145.80, 136.70, 130.92, 125.14, 125.06, 124.78, 124.47, 113.04, 112.73, 112.09, 109.00, 96.14, 84.82, 23.45, 21.56. HPLC purity: 96.28%. HRMS (ESI): *m/z* calculated for C₂₁H₁₆N₅ [M + H]⁺: 338.1406. Found: 338.1393.

11-(Pyridin-4-ylethynyl)-5,6,7,8-tetrahydropyrimido[4',5':3,4]cyclohepta[1,2-*b*]indol-2-amine (5). The reaction was carried out according to general procedure D using **43** (187 mg, 0.57 mmol), 4-ethynylpyridine (117 mg, 1.14 mmol), TEA (115 mg, 1.14 mmol), Pd(PPh₃)₄ (66 mg, 60 μmol), and CuI (13 mg, 60 μmol) in DMF (1.5 mL) at 100 °C overnight to afford the title compound (7.5 mg, 3.8% yield). ¹H NMR (850 MHz, CD₃OD-*d*₄) δ 8.95–8.91 (m, 1H), 8.55–8.49 (m, 2H), 7.91 (s, 1H), 7.57–7.53 (m, 2H), 7.39–7.33 (m, 2H), 3.27–3.22 (m, 2H), 2.75–2.72 (m, 2H), 2.12–2.06 (m, 2H). ¹³C NMR (214 MHz, CD₃OD-*d*₄) δ 164.16, 163.18, 156.81, 150.11, 146.25, 138.32, 134.93, 129.07, 128.68, 127.13, 127.01, 123.03, 114.58, 112.22, 111.72, 98.97, 85.10, 31.22, 30.77, 25.66. HPLC purity: 96.99%. HRMS (ESI): *m/z* calculated for C₂₂H₁₈N₅ [M + H]⁺: 352.1562. Found: 352.1556.

12-(Pyridin-4-ylethynyl)-6,7,8,9-tetrahydro-5H-pyrimido[4',5':3,4]cycloocta[1,2-*b*]indol-2-amine (6). The reaction was carried out according to general procedure D using **44** (188 mg, 0.55 mmol), 4-ethynylpyridine (85 mg, 0.82 mmol), TEA (111 mg, 1.1 mmol), Pd(PPh₃)₄ (32 mg, 30 μmol), and CuI (6.0 mg, 30 μmol) in DMA (1.0 mL) at 100 °C overnight to afford the title compound (15.9 mg, 8.0% yield). ¹H NMR (850 MHz, CD₃OD-*d*₄) δ 8.50 (d, *J* = 5.2 Hz, 2H), 8.12–8.08 (m, 2H), 7.50–7.47 (m, 2H), 7.34 (dd, *J* = 3.8, 1.2 Hz, 2H), 3.08–3.04 (m, 2H), 2.66–2.61 (m, 2H), 1.88–1.79 (m, 4H). ¹³C NMR (214 MHz, CD₃OD-*d*₄) δ 164.80, 163.15, 159.25, 150.11, 143.81, 137.93, 134.80, 129.27, 126.93, 126.69, 126.07, 125.67, 114.16, 111.86, 110.63, 98.63, 85.10, 32.22, 29.00, 28.19. HPLC purity: 97.95%. HRMS (ESI): *m/z* calculated for C₂₃H₂₀N₅ [M + H]⁺: 366.1719. Found: 366.1711.

1-(2-Amino-6,7-dihydro-5H-pyrimido[5,4-*c*]carbazol-10-yl)-4-methylpent-1-yn-3-ol (10). The reaction was carried out according to general procedure D using **42** (142 mg, 0.45 mmol), 4-methylpent-1-yn-3-ol (89 mg, 0.90 mmol), TEA (91 mg, 0.9 mmol), Pd(PPh₃)₄ (58 mg, 45 μmol), and CuI (17 mg, 90 μmol) in DMF (1.5 mL) at 100 °C overnight to afford the title compound (14 mg, 9.0% yield). ¹H NMR (400 MHz, CD₃OD-*d*₄) δ 8.42 (dd, *J* = 1.7, 0.8 Hz, 1H), 7.72 (d, *J* = 1.2 Hz, 1H), 7.39 (dd, *J* = 8.4, 0.8 Hz, 1H), 7.32 (dd, *J* = 8.4, 1.6 Hz, 1H), 4.33 (d, *J* = 5.9 Hz, 1H), 3.14 (td, *J* = 7.3, 1.2 Hz, 2H), 3.03 (dd, *J* = 8.3, 6.8 Hz, 2H), 1.93 (dq, *J* = 13.2, 6.7 Hz, 1H), 1.09 (dd, *J* = 11.0, 6.7 Hz, 6H). ¹³C NMR (101 MHz, CD₃OD-*d*₄) δ 167.82, 156.71, 153.45, 138.47, 137.89, 128.34, 126.07, 125.92, 118.46, 116.40, 113.08, 110.61, 88.82, 86.81, 69.05, 36.20, 22.69, 22.43, 18.84, 18.27. HPLC purity: 95.34%. HRMS (ESI): *m/z* calculated for C₂₀H₂₁N₅ [M + H]⁺: 333.1715. Found: 333.1703.

1-(2-Amino-5,6,7,8-tetrahydropyrimido[4',5':3,4]cyclohepta[1,2-*b*]indol-11-yl)-4-methylpent-1-yn-3-ol (11). The reaction was carried out according to general procedure D using **43** (190 mg, 0.58 mmol), 4-methylpent-1-yn-3-ol (113 mg, 1.16 mmol), TEA (175 mg, 1.73 mmol), Pd(PPh₃)₄ (67 mg, 60 μmol), and CuI (15 mg, 60 μmol) in DMF (1.5 mL) at 100 °C overnight to afford the title compound (4.0 mg, 2% yield). ¹H NMR (400 MHz, CD₃OD-*d*₄) δ 8.83 (t, *J* = 1.1 Hz, 1H), 7.75 (s, 1H), 7.29 (d, *J* = 0.9 Hz, 2H), 4.35 (d, *J* = 5.9 Hz, 1H), 3.30–3.25 (m, 2H), 2.83–2.76 (m, 2H), 2.09 (dt, *J* = 10.3, 6.3 Hz, 2H), 1.92 (dt, *J* = 13.2, 6.6 Hz, 1H), 1.09 (dd, *J* = 10.8, 6.7 Hz, 6H). ¹³C NMR (101 MHz, CD₃OD-*d*₄) δ 170.63, 155.39, 151.96, 140.98, 137.68, 128.82, 128.27, 128.17, 122.73, 117.81, 112.15, 111.95, 88.36, 87.53, 69.13, 36.24, 31.37, 31.28, 23.86, 18.82, 18.29. HPLC purity: 95.56%. HRMS (ESI): *m/z* calculated for C₂₁H₂₃N₄O [M + H]⁺: 347.1872. Found: 347.1867.

10-((1-Methyl-1H-imidazol-5-yl)ethynyl)-6,7-dihydro-5H-pyrimido[5,4-*c*]carbazol-2-amine (14). The reaction was carried out according to general procedure D using **42** (139 mg, 0.44 mmol), 5-ethynyl-1-methyl-1H-imidazole (94 mg, 0.88 mmol), TEA (90 mg, 0.88 mmol), Pd(PPh₃)₄ (51 mg, 44 μmol), and CuI (17 mg, 88 μmol) in DMF (1.5 mL) at 100 °C overnight to afford the title compound (16 mg, 12% yield). ¹H NMR (600 MHz, DMSO-*d*₆) δ 11.87 (s, 1H), 8.45 (d, *J* = 1.6 Hz, 1H), 7.93 (s, 1H), 7.77 (s, 1H), 7.43 (d, *J* = 8.3 Hz, 1H), 7.30 (dd, *J* = 8.3, 1.7 Hz, 1H), 7.28 (s, 1H), 6.22 (s, 2H), 3.74 (s, 3H), 3.00 (t, *J* = 7.8 Hz, 2H), 2.85 (t, *J* = 7.8 Hz, 2H). ¹³C NMR (214 MHz, CD₃OD-*d*₄) δ 163.88, 162.89, 153.57, 147.68, 139.69, 138.35, 133.09, 126.41, 126.14, 125.90, 118.56, 115.72, 115.70, 112.64, 110.65, 99.26,

74.99, 32.50, 25.16, 22.93. HPLC purity: 98.86%. HRMS (ESI): m/z calculated for $C_{20}H_{16}N_6Na$ $[M + Na]^+$: 363.1334. Found: 363.1347.

10-(Cyclopropylethynyl)-6,7-dihydro-5H-pyrimido[5,4-c]-carbazol-2-amine (15). The reaction was carried out according to general procedure D using **42** (157 mg, 0.50 mmol), ethynylcyclopropane (66 mg, 1.0 mmol), TEA (101 mg, 1.0 mmol), Pd(PPh₃)₄ (58 mg, 50 μmol), and CuI (19 mg, 100 μmol) in DMF (1.5 mL) at 100 °C overnight to afford the title compound (5.0 mg, 3.0% yield). ¹H NMR (700 MHz, CD₃OD-*d*₄) δ 8.34 (d, *J* = 1.7 Hz, 1H), 7.74 (s, 1H), 7.31 (d, *J* = 8.3 Hz, 1H), 7.21 (dd, *J* = 8.4, 1.6 Hz, 1H), 3.10 (t, *J* = 7.6 Hz, 2H), 2.99 (t, *J* = 7.6 Hz, 2H), 1.49–1.44 (m, 1H), 0.88 (dt, *J* = 8.1, 3.3 Hz, 2H), 0.74 (dt, *J* = 4.7, 3.1 Hz, 2H). ¹³C NMR (214 MHz, CD₃OD-*d*₄) δ 166.59, 158.44, 151.76, 141.63, 137.91, 127.87, 125.99, 125.93, 119.03, 116.19, 112.72, 110.50, 92.23, 77.57, 24.82, 22.54, 8.86. HPLC purity: 96.33%. HRMS (ESI): m/z calculated for $C_{19}H_{17}N_4$ $[M + H]^+$: 301.1453. Found: 301.1445.

10-(3-(Dimethylamino)prop-1-yn-1-yl)-6,7-dihydro-5H-pyrimido[5,4-c]carbazol-2-amine (16). The reaction was carried out according to general procedure D using **42** (99 mg, 0.30 mmol), *N,N*-dimethylprop-2-yn-1-amine (79 mg, 0.9 mmol), DIPA (64 mg, 0.63 mmol), Pd(PPh₃)₄ (37 mg, 32 μmol), and CuI (13 mg, 64 μmol) in DMF (1.5 mL) at 100 °C overnight to afford the title compound (4.7 mg, 4.7% yield). ¹H NMR (700 MHz, CD₃OD-*d*₄) δ 8.54 (d, *J* = 2.1 Hz, 1H), 7.77 (d, *J* = 2.1 Hz, 1H), 7.47 (dd, *J* = 8.4, 2.1 Hz, 1H), 7.43 (d, *J* = 8.3 Hz, 1H), 4.34 (s, 2H), 3.17 (t, *J* = 7.6, 2.0 Hz, 2H), 3.07–3.03 (m, 8H). ¹³C NMR (214 MHz, CD₃OD-*d*₄) δ 164.25, 161.84, 149.41, 149.23, 138.55, 127.20, 126.42, 126.02, 115.97, 115.69, 112.78, 110.58, 90.73, 78.97, 43.51, 25.00, 22.76. HPLC purity: 100%. HRMS (ESI): m/z calculated for $C_{19}H_{20}N_5$ $[M + H]^+$: 218.1719. Found: 318.1713.

11-(3-(Dimethylamino)prop-1-yn-1-yl)-5,6,7,8-tetrahydropyrimido[4',5':3,4]cyclohepta[1,2-b]indol-2-amine (17). The reaction was carried out according to general procedure D using **43** (199 mg, 0.6 mmol), *N,N*-dimethylprop-2-yn-1-amine (201 mg, 2.41 mmol), TEA (122 mg, 1.21 mmol), Pd(PPh₃)₄ (35 mg, 30 μmol), and CuI (7.0 mg, 30 μmol) in DMF (1.5 mL) at 100 °C overnight to afford the title compound (2.9 mg, 1.5% yield). ¹H NMR (700 MHz, CD₃OD-*d*₄) δ 8.85 (s, 1H), 7.93–7.85 (m, 1H), 7.33–7.24 (m, 2H), 4.00 (s, 2H), 3.24 (t, *J* = 6.6 Hz, 2H), 2.80 (s, 6H), 2.75–2.72 (m, 2H), 2.09 (dt, *J* = 10.4, 6.4 Hz, 2H). ¹³C NMR (126 MHz, CD₃OD-*d*₄) δ 164.62, 162.58, 155.68, 146.62, 138.08, 128.93, 128.47, 127.02, 123.11, 114.46, 112.05, 111.61, 91.82, 77.90, 43.38, 31.18, 30.77, 25.54, 18.35. HPLC purity: 100%. HRMS (ESI): m/z calculated for $C_{20}H_{22}N_5$ $[M + H]^+$: 332.1875. Found: 332.1868.

12-((1-Methyl-1H-imidazol-5-yl)ethynyl)-6,7,8,9-tetrahydro-5H-pyrimido[4',5':3,4]cycloocta[1,2-b]indol-2-amine (27). The reaction was carried out according to general procedure D using **44** (186 mg, 0.54 mmol), 5-ethynyl-1-methyl-1H-imidazole (86 mg, 0.81 mmol), TEA (110 mg, 1.1 mmol), Pd(PPh₃)₄ (31 mg, 30 μmol), and CuI (6.0 mg, 30 μmol) in DMA (1.0 mL) at 100 °C overnight to afford the title compound (31 mg, 16% yield). ¹H NMR (500 MHz, DMSO-*d*₆) δ 11.48 (s, 1H), 8.06 (d, *J* = 4.7 Hz, 2H), 7.74 (s, 1H), 7.32 (d, *J* = 8.3 Hz, 1H), 7.24 (dd, *J* = 7.6, 2.1 Hz, 2H), 6.35 (s, 2H), 3.70 (s, 3H), 3.03–2.98 (m, 2H), 1.75–1.71 (m, 4H). ¹³C NMR (126 MHz, DMSO-*d*₆) δ 162.25, 161.87, 158.22, 141.87, 138.98, 135.52, 132.91, 127.76, 124.43, 123.89, 112.25, 110.79, 109.35, 97.95, 31.62, 30.78, 27.60. HPLC purity: 100%. HRMS (ESI): m/z calculated for $C_{22}H_{21}N_6$ $[M + Na]^+$: 369.1828. Found: 369.1822.

12-(Cyclopropylethynyl)-6,7,8,9-tetrahydro-5H-pyrimido[4',5':3,4]cycloocta[1,2-b]indol-2-amine (28). The reaction was carried out according to general procedure D using **44** (209 mg, 0.61 mmol), ethynylcyclopropane (81 mg, 1.22 mmol), TEA (136 mg, 1.34 mmol), Pd(PPh₃)₄ (35 mg, 30 μmol), and CuI (6.0 mg, 30 μmol) in DMA (1.0 mL) at 100 °C overnight to afford the title compound (7.7 mg, 3.9% yield). ¹H NMR (850 MHz, CD₃OD-*d*₄) δ 8.08 (s, 1H), 7.84–7.82 (m, 1H), 7.20 (dd, *J* = 8.3, 0.7 Hz, 1H), 7.10 (dd, *J* = 8.3, 1.6 Hz, 1H), 3.06–3.01 (m, 2H), 2.66–2.60 (m, 2H), 1.84 (d, *J* = 5.7 Hz, 4H), 1.43 (tt, *J* = 8.2, 5.0 Hz, 1H), 0.85–0.80 (m, 2H), 0.70–0.67 (m, 2H). ¹³C NMR (214 MHz, CD₃OD-*d*₄) δ 165.45, 162.48, 158.29, 143.53, 136.78, 129.03, 126.63, 124.47, 116.76, 113.61, 111.36, 110.10, 91.07, 78.20, 32.25, 28.99, 8.79, 0.82. HPLC purity: 97.53%. HRMS

(ESI): m/z calculated for $C_{21}H_{21}N_4$ $[M + H]^+$: 329.1766. Found: 329.1758.

12-(3-(Dimethylamino)prop-1-yn-1-yl)-6,7,8,9-tetrahydro-5H-pyrimido[4',5':3,4]cycloocta[1,2-b]indol-2-amine (29). The reaction was carried out according to general procedure D using **44** (99 mg, 0.29 mmol), *N,N*-dimethylprop-2-yn-1-amine (120 mg, 1.45 mmol), DIPA (59 mg, 0.58 mmol), Pd(PPh₃)₄ (34 mg, 30 μmol), and CuI (6.0 mg, 30 μmol) in DMA (1.0 mL) at 100 °C overnight to afford the title compound (4.6 mg, 4.6% yield). ¹H NMR (700 MHz, CD₃OD-*d*₄) δ 8.20 (s, 1H), 8.14 (s, 1H), 7.38–7.32 (m, 2H), 4.30 (s, 2H), 3.19–3.14 (m, 2H), 3.02 (s, 6H), 2.78–2.73 (m, 2H), 1.94–1.88 (m, 4H). ¹³C NMR (176 MHz, CD₃OD-*d*₄) δ 156.06, 148.65, 138.01, 130.77, 128.87, 127.62, 125.97, 122.99, 116.86, 115.25, 114.43, 112.29, 93.01, 75.94, 42.72, 31.84, 29.20, 27.84, 22.03. HPLC purity: 95.61%. HRMS (ESI): m/z calculated for $C_{21}H_{24}N_5$ $[M + H]^+$: 346.2032. Found: 346.2024.

General Procedure for the Synthesis of Compounds 18–26: Procedure E. A mixture of **43** (1 equiv), alkyne (3–3.5 equiv), and DIPA (2–2.5 equiv) in propanol (0.2–0.3 M) was degassed, followed by addition of PdCl₂(PPh₃)₂ (0.1 equiv) and CuI (0.1 equiv). The reaction mixture was heated to 100 °C and stirred overnight. After completion of the reaction, the mixture was cooled to r.t., diluted with EtOAc, and passed through a thin pad of celite. The filtrate was concentrated *in vacuo* and the crude residue was purified by preparative HPLC (10–100% MeOH in H₂O + 0.1% TFA) to give the title compounds.

***N*-(4-(2-Amino-5,6,7,8-tetrahydropyrimido[4',5':3,4]cyclohepta[1,2-b]indol-11-yl)-2-methylbut-3-yn-2-yl)acetamide (18).** The reaction was carried out according to general procedure D using **43** (264 mg, 0.7 mmol), *N*-(2-methylbut-3-yn-2-yl)acetamide (302 mg, 2.4 mmol), DIPA (163 mg, 1.61 mmol), Pd(PPh₃)₂Cl₂ (56 mg, 80 μmol), and CuI (13 mg, 80 μmol) in propanol (3.0 mL) at 100 °C overnight to afford the title compound (24 mg, 8.0% yield). ¹H NMR (600 MHz, DMSO-*d*₆) δ 11.59 (s, 1H), 8.73 (d, *J* = 1.6 Hz, 1H), 7.97 (s, 1H), 7.92 (s, 1H), 7.25 (d, *J* = 8.3 Hz, 1H), 7.09 (dd, *J* = 8.2, 1.6 Hz, 1H), 6.21 (s, 2H), 3.15 (t, *J* = 6.6 Hz, 2H), 2.64–2.59 (m, 2H), 1.95–1.90 (m, 2H), 1.83 (s, 3H), 1.62 (s, 6H). ¹³C NMR (214 MHz, CD₃OD-*d*₄) δ 172.49, 166.32, 160.72, 147.68, 137.50, 135.99, 128.84, 128.00, 127.48, 116.73, 112.07, 111.40, 91.03, 83.73, 31.29, 30.93, 29.79, 25.12, 23.99, 23.40. HPLC purity: 97.62%. HRMS (ESI): m/z calculated for $C_{22}H_{24}N_5O$ $[M + H]^+$: 374.1981. Found: 374.1975.

***N*-(4-(2-Amino-5,6,7,8-tetrahydropyrimido[4',5':3,4]cyclohepta[1,2-b]indol-11-yl)-2-methylbut-3-yn-2-yl)methanesulfonamide (19).** The reaction was carried out according to general procedure D using **43** (241 mg, 0.73 mmol), *N*-(2-methylbut-3-yn-2-yl)-methanesulfonamide (354 mg, 2.2 mmol), DIPA (148 mg, 1.47 mmol), Pd(PPh₃)₂Cl₂ (51 mg, 70 μmol), and CuI (12 mg, 70 μmol) in propanol (3.0 mL) at 100 °C overnight to afford the title compound (36 mg, 12% yield). ¹H NMR (600 MHz, DMSO-*d*₆) δ 11.65 (s, 1H), 8.77 (d, *J* = 1.6 Hz, 1H), 8.16 (s, 1H), 7.90 (d, *J* = 7.0 Hz, 1H), 7.45 (s, 1H), 7.29 (d, *J* = 8.2 Hz, 1H), 7.14 (dd, *J* = 8.2, 1.7 Hz, 1H), 6.18 (s, 2H), 3.18 (td, *J* = 6.6, 3.5 Hz, 2H), 3.15 (s, 3H), 2.62–2.59 (m, 2H), 1.94 (dt, *J* = 11.1, 6.1 Hz, 2H), 1.62 (s, 6H). ¹³C NMR (151 MHz, DMSO-*d*₆) δ 162.05, 161.00, 156.85, 156.78, 144.30, 135.75, 127.34, 126.61, 124.85, 120.33, 110.64, 110.43, 89.68, 84.55, 49.41, 41.99, 40.43, 31.18, 24.05. HPLC purity: 95.31%. HRMS (ESI): m/z calculated for $C_{21}H_{24}N_5O_2S$ $[M + H]^+$: 410.1651. Found: 410.1645.

11-(3-Methoxy-3-methylbut-1-yn-1-yl)-5,6,7,8-tetrahydropyrimido[4',5':3,4]cyclohepta[1,2-b]indol-2-amine (20). The reaction was carried out according to general procedure E using **43** (285 mg, 0.87 mmol), 3-methoxy-3-methylbut-1-yne (255 mg, 2.6 mmol), DIPA (175 mg, 1.73 mmol), PdCl₂(PPh₃)₂ (61 mg, 80 μmol), and CuI (13 mg, 80 μmol) in propanol (3.0 mL) at 100 °C overnight to afford the title compound (45 mg, 15% yield). ¹H NMR (500 MHz, DMSO-*d*₆) δ 11.64 (s, 1H), 8.76 (s, 1H), 7.26 (d, *J* = 8.2 Hz, 1H), 7.14 (d, *J* = 8.3 Hz, 1H), 6.31 (s, 2H), 3.34 (s, 3H), 3.15 (t, *J* = 6.5 Hz, 2H), 2.63 (d, *J* = 8.1 Hz, 2H), 1.98–1.90 (m, 2H), 1.50 (s, 6H). ¹³C NMR (126 MHz, DMSO-*d*₆) δ 161.09, 144.22, 135.70, 127.24, 126.68, 125.39, 113.21, 110.53, 88.48, 86.04, 70.44, 50.97, 29.75, 29.52, 28.42,

24.13. HPLC purity: 98.7%. HRMS (ESI): m/z calculated for $C_{21}H_{23}N_4O$ $[M + H]^+$: 347.1872. Found: 347.1863.

4-(2-Amino-5,6,7,8-tetrahydropyrimido[4',5':3,4]cyclohepta[1,2-b]indol-11-yl)but-3-yn-2-ol (21). The reaction was carried out according to general procedure E using **43** (310 mg, 0.94 mmol), but-3-yn-2-ol (198 mg, 2.82 mmol), DIPA (168 mg, 1.67 mmol), $PdCl_2(PPh_3)_2$ (66 mg, 90 μ mol), and CuI (20 mg, 90 μ mol) in propanol (3.0 mL) at 100 °C overnight to afford the title compound (8.2 mg, 2.7% yield). 1H NMR (850 MHz, CD_3OD-d_4) δ 8.77 (s, 1H), 7.88 (s, 1H), 7.25 (dd, $J = 8.3$, 0.7 Hz, 1H), 7.20 (dd, $J = 8.3$, 1.6 Hz, 1H), 4.71 (q, $J = 6.6$ Hz, 1H), 3.22 (t, $J = 6.6$ Hz, 2H), 2.73–2.70 (m, 2H), 2.07 (dt, $J = 11.0$, 6.6 Hz, 2H), 1.51 (d, $J = 6.6$ Hz, 3H). ^{13}C NMR (214 MHz, CD_3OD-d_4) δ 164.34, 163.10, 156.62, 145.85, 137.57, 128.90, 127.80, 126.77, 123.01, 115.88, 111.94, 111.32, 89.55, 86.39, 59.30, 31.21, 30.70, 25.71, 25.00. HPLC purity: 100%. HRMS (ESI): m/z calculated for $C_{19}H_{19}N_4O$ $[M + H]^+$: 319.1559. Found: 319.1553.

4-(2-Amino-5,6,7,8-tetrahydropyrimido[4',5':3,4]cyclohepta[1,2-b]indol-11-yl)but-3-yn-1-ol (22). The reaction was carried out according to general procedure E using **43** (310 mg, 0.94 mmol), but-3-yn-1-ol (198 mg, 2.8 mmol), DIPA (191 mg, 1.89 mmol), $PdCl_2(PPh_3)_2$ (66 mg, 90 μ mol), and CuI (15 mg, 90 μ mol) in propanol (3.0 mL) at 100 °C overnight to afford the title compound (7.2 mg, 2.4% yield). 1H NMR (850 MHz, CD_3OD-d_4) δ 8.74 (s, 1H), 7.87 (s, 1H), 7.22 (dd, $J = 8.2$, 0.7 Hz, 1H), 7.18 (dd, $J = 8.2$, 1.6 Hz, 1H), 3.75 (t, $J = 6.9$ Hz, 2H), 3.21 (t, $J = 6.6$ Hz, 2H), 2.73–2.69 (m, 2H), 2.63 (t, $J = 6.8$ Hz, 2H), 2.07 (dt, $J = 10.9$, 6.6 Hz, 2H). ^{13}C NMR (214 MHz, CD_3OD-d_4) δ 164.20, 162.92, 156.40, 145.50, 137.09, 128.68, 127.48, 126.72, 122.76, 116.61, 111.69, 110.99, 84.35, 84.22, 61.87, 31.04, 30.51, 25.54, 24.20. HPLC purity: 100%. HRMS (ESI): m/z calculated for $C_{19}H_{19}N_4O$ $[M + H]^+$: 319.1559. Found: 319.1553.

4-(2-Amino-5,6,7,8-tetrahydropyrimido[4',5':3,4]cyclohepta[1,2-b]indol-11-yl)-2,2-dimethylbut-3-yn-1-ol (23). The reaction was carried out according to general procedure E using **43** (285 mg, 0.87 mmol), 2-methylpent-4-yn-2-ol (255 mg, 2.6 mmol), DIPA (175 mg, 1.73 mmol), $PdCl_2(PPh_3)_2$ (61 mg, 90 μ mol), and CuI (15 mg, 90 μ mol) in propanol (3.0 mL) at 100 °C overnight to afford the title compound (12.6 mg, 4.0% yield). 1H NMR (850 MHz, CD_3OD-d_4) δ 8.71 (s, 1H), 7.84 (s, 1H), 7.22 (dd, $J = 8.2$, 0.7 Hz, 1H), 7.19 (dd, $J = 8.3$, 1.6 Hz, 1H), 3.51 (s, 2H), 3.21 (t, $J = 6.5$ Hz, 2H), 2.74–2.69 (m, 2H), 2.09–2.04 (m, 2H), 1.30 (s, 6H). ^{13}C NMR (214 MHz, CD_3OD-d_4) δ 165.55, 161.71, 153.74, 146.75, 137.26, 128.81, 127.50, 127.36, 122.93, 117.19, 111.95, 111.29, 93.36, 83.91, 72.09, 40.44, 35.17, 31.23, 30.76, 26.23, 25.47, 25.35. HPLC purity: 98.28%. HRMS (ESI): m/z calculated for $C_{21}H_{23}N_4O$ $[M + H]^+$: 347.1872. Found: 347.1868.

5-(2-Amino-5,6,7,8-tetrahydropyrimido[4',5':3,4]cyclohepta[1,2-b]indol-11-yl)-2-methylpent-4-yn-2-ol (24). The reaction was carried out according to general procedure E using **43** (285 mg, 0.87 mmol), 2-methylpent-4-yn-2-ol (255 mg, 2.6 mmol), DIPA (175 mg, 1.73 mmol), $PdCl_2(PPh_3)_2$ (61 mg, 90 μ mol), and CuI (15 mg, 90 μ mol) in propanol (3.0 mL) at 100 °C overnight to afford the title compound (19 mg, 6.3% yield). 1H NMR (600 MHz, $DMSO-d_6$) δ 11.57 (s, 1H), 8.72 (s, 1H), 8.18 (s, 1H), 7.91 (s, 1H), 7.25 (d, $J = 8.2$ Hz, 1H), 7.13 (d, $J = 8.3$ Hz, 1H), 6.19 (s, 2H), 3.17 (t, $J = 6.7$ Hz, 2H), 2.64–2.61 (m, 2H), 1.99–1.93 (m, 2H), 1.27 (s, 6H). ^{13}C NMR (214 MHz, CD_3OD-d_4) δ 166.19, 160.43, 151.36, 147.46, 137.11, 128.66, 127.56, 127.13, 122.70, 117.32, 111.76, 111.20, 84.95, 84.92, 71.13, 40.24, 35.38, 31.06, 30.71, 28.74, 24.95. HPLC purity: 95.86%. HRMS (ESI): m/z calculated for $C_{21}H_{23}N_4O$ $[M + H]^+$: 347.1872. Found: 347.1865.

1-(2-Amino-5,6,7,8-tetrahydropyrimido[4',5':3,4]cyclohepta[1,2-b]indol-11-yl)-3-methylpent-1-yn-3-ol (25). The reaction was carried out according to general procedure E using **43** (143 mg, 0.43 mmol), 3-methylpent-1-yn-3-ol (127 mg, 1.3 mmol), DIPA (88 mg, 0.87 mmol), $PdCl_2(PPh_3)_2$ (30 mg, 40 μ mol), and CuI (7.0 mg, 40 μ mol) in propanol (3.0 mL) at 100 °C overnight to afford the title compound (14.6 mg, 9.7% yield). 1H NMR (600 MHz, $DMSO-d_6$) δ 11.61 (s, 1H), 8.69 (d, $J = 1.6$ Hz, 1H), 8.27 (s, 1H), 7.92 (s, 1H), 7.25 (d, $J = 8.3$ Hz, 1H), 7.10 (dd, $J = 8.3$, 1.6 Hz, 1H), 6.17 (s, 2H), 3.15 (t, $J = 6.6$ Hz, 2H), 2.61 (d, $J = 5.0$ Hz, 2H), 1.94 (dt, $J = 11.3$, 6.3 Hz, 2H), 1.72–1.59 (m, $J = 7.0$, 6.5 Hz, 2H), 1.45 (s, 3H), 1.02 (t, $J = 7.4$ Hz, 3H). ^{13}C NMR (214 MHz, CD_3OD-d_4) δ 166.22, 160.87, 152.09, 147.58, 137.55,

128.85, 127.70, 127.24, 123.00, 116.59, 112.00, 111.51, 91.44, 85.91, 69.78, 37.87, 31.19, 30.84, 29.69, 9.57. HPLC purity: 100%. HRMS (ESI): m/z calculated for $C_{21}H_{23}N_4O$ $[M + H]^+$: 347.1872. Found: 347.1860.

1-(2-Amino-5,6,7,8-tetrahydropyrimido[4',5':3,4]cyclohepta[1,2-b]indol-11-yl)-3-ethylpent-1-yn-3-ol (26). The reaction was carried out according to general procedure E using **43** (274 mg, 0.83 mmol), 3-ethylpent-1-yn-3-ol (280 mg, 2.5 mmol), DIPA (168 mg, 1.67 mmol), $PdCl_2(PPh_3)_2$ (58 mg, 80 μ mol), and CuI (13 mg, 80 μ mol) in propanol (3.0 mL) at 100 °C overnight to afford the title compound (46.2 mg, 15% yield). 1H NMR (500 MHz, $DMSO-d_6$) δ 11.61 (s, 1H), 8.71 (s, 1H), 7.25 (d, $J = 8.1$ Hz, 1H), 7.11 (d, $J = 7.6$ Hz, 1H), 6.21 (s, 2H), 3.15 (t, $J = 6.6$ Hz, 2H), 2.62 (d, $J = 6.7$ Hz, 2H), 2.00–1.92 (s, 2H), 1.64 (qd, $J = 13.7$, 6.8 Hz, 4H), 1.01 (t, $J = 7.4$ Hz, 6H). ^{13}C NMR (126 MHz, $DMSO-d_6$) δ 161.23, 144.13, 135.50, 127.22, 126.36, 125.32, 113.99, 110.49, 90.86, 84.88, 34.18, 29.66, 29.40, 24.26, 8.80. HPLC purity: 100%. HRMS (ESI): m/z calculated for $C_{22}H_{25}N_4O$ $[M + H]^+$: 361.2028. Found: 361.2026.

General Procedure for the Synthesis of Compounds 7–9, 12, and 13: Procedure F. A mixture of **42–44** (1 equiv), boronic acid (1.2–1.6 equiv), and K_2CO_3 (2 equiv) in a mixture of dioxane (0.2–0.3 M) and water (1.0–2.0 M) was degassed, followed by addition of $Pd(PPh_3)_4$ (0.05 equiv). The reaction mixture was heated to 95 °C and allowed to stir overnight. After completion of the reaction, the mixture was cooled to r.t. and diluted with EtOAc and water. The organic layer was washed with water and concentrated *in vacuo*. The crude residue was purified via preparative HPLC (10–100% MeOH in H_2O + 0.1% TFA) to afford the title compounds.

10-(4-Fluorophenyl)-6,7-dihydro-5H-pyrimido[5,4-c]carbazol-2-amine (7). The reaction was carried out according to general procedure F using **42** (95 mg, 0.30 mmol), 4-fluorophenylboronic acid (64 mg, 0.47 mmol), K_2CO_3 (64 mg, 0.63 mmol), and $Pd(PPh_3)_4$ (18 mg, 15 μ mol) in a mixture of dioxane/water (2.0 mL/0.3 mL) at 95 °C overnight to afford the title compound (29 mg, 29% yield). 1H NMR (500 MHz, $DMSO-d_6$) δ 11.69 (s, 1H), 8.50 (s, 1H), 7.91 (s, 1H), 7.71 (dd, $J = 8.4$, 5.4 Hz, 2H), 7.45 (d, $J = 8.4$ Hz, 1H), 7.39 (dd, $J = 8.3$, 1.9 Hz, 1H), 7.27 (t, $J = 8.7$ Hz, 2H), 6.18 (s, 2H), 2.99 (t, $J = 7.7$ Hz, 2H), 2.85 (t, $J = 7.8$ Hz, 2H). ^{13}C NMR (126 MHz, $DMSO-d_6$) δ 162.64, 160.32, 160.11, 153.53, 145.18, 138.20, 135.94, 131.90, 128.66, 128.59, 125.14, 120.69, 118.76, 115.49, 115.32, 113.00, 111.78, 109.12, 23.62, 21.69. HPLC purity: 100%. HRMS (ESI): m/z calculated for $C_{20}H_{16}FN_4$ $[M + H]^+$: 331.1359. Found: 331.1352.

11-(4-Fluorophenyl)-5,6,7,8-tetrahydropyrimido[4',5':3,4]cyclohepta[1,2-b]indol-2-amine (8). The reaction was carried out according to general procedure F using **43** (192 mg, 0.58 mmol), 4-fluorophenylboronic acid (122 mg, 0.87 mmol), K_2CO_3 (161 mg, 1.16 mmol), and $Pd(PPh_3)_4$ (34 mg, 29 μ mol) in a mixture of dioxane/water (2.0 mL/0.3 mL) at 95 °C overnight to afford the title compound (22.7 mg, 44% yield). 1H NMR (600 MHz, $DMSO-d_6$) δ 11.51 (s, 1H), 8.94 (d, $J = 1.8$ Hz, 1H), 7.92 (s, 1H), 7.75 (dd, $J = 8.5$, 5.6 Hz, 2H), 7.41–7.33 (m, 2H), 7.22 (t, $J = 8.8$ Hz, 2H), 6.22 (s, 2H), 3.18 (t, $J = 6.6$ Hz, 2H), 2.65–2.60 (m, 2H), 1.96 (dt, $J = 11.8$, 6.4 Hz, 2H). ^{13}C NMR (214 MHz, CD_3OD-d_4) δ 164.68, 163.89, 163.12, 162.76, 156.52, 145.59, 140.67, 140.65, 137.43, 134.15, 129.98, 129.94, 129.51, 122.70, 122.18, 116.23, 116.13, 112.19, 111.61, 31.13, 30.60, 26.04. HPLC purity: 100%. HRMS (ESI): m/z calculated for $C_{21}H_{18}FN_4$ $[M + H]^+$: 345.1515. Found: 345.1511.

12-(4-Fluorophenyl)-6,7,8,9-tetrahydro-5H-pyrimido[4',5':3,4]cycloocta[1,2-b]indol-2-amine (9). The reaction was carried out according to general procedure F using **44** (144 mg, 0.42 mmol), 4-fluorophenylboronic acid (70 mg, 0.50 mmol), K_2CO_3 (116 mg, 0.84 mmol), and $Pd(PPh_3)_4$ (24 mg, 21 μ mol) in a mixture of dioxane/water (2.0 mL/0.3 mL) at 95 °C overnight to afford the title compound (48 mg, 32% yield). 1H NMR (500 MHz, $DMSO-d_6$) δ 11.28 (s, 1H), 8.06 (d, $J = 16.4$ Hz, 2H), 7.64 (dd, $J = 8.7$, 5.6 Hz, 2H), 7.32 (q, $J = 8.4$ Hz, 2H), 7.21 (t, $J = 8.8$ Hz, 2H), 6.30 (s, 2H), 3.02–2.96 (m, 2H), 2.54–2.49 (m, 2H), 1.74 (s, 4H). ^{13}C NMR (126 MHz, $DMSO-d_6$) δ 162.32, 162.23, 162.11, 160.18, 158.08, 141.28, 138.67, 138.64, 135.10, 130.78, 128.53, 128.46, 128.43, 120.42, 118.59, 115.45, 115.29, 110.67, 109.58,

30.93, 27.66, 26.77. HPLC purity: 100%. HRMS (ESI): m/z calculated for $C_{22}H_{20}FN_4$ $[M + H]^+$: 359.1672. Found: 359.1668.

10-(1-Methyl-1H-pyrazol-4-yl)-6,7-dihydro-5H-pyrimido[5,4-c]-carbazol-2-amine (12). The reaction was carried out according to general procedure F using **42** (100 mg, 0.32 mmol), (1-methyl-1H-pyrazol-4-yl)boronic acid (99 mg, 0.47 mmol), K_2CO_3 (64 mg, 0.63 mmol), and $Pd(PPh_3)_4$ (18 mg, 15 μ mol) in a mixture of dioxane/water (2.0 mL/0.3 mL) at 95 °C overnight to afford the title compound (36 mg, 36% yield). 1H NMR (500 MHz, $DMSO-d_6$) δ 11.56 (s, 1H), 8.45 (s, 1H), 8.07 (s, 1H), 7.89 (d, $J = 2.3$ Hz, 2H), 7.37–7.28 (m, 2H), 6.21 (s, 2H), 3.88 (s, 3H), 2.97 (t, $J = 7.7$ Hz, 2H), 2.84 (t, $J = 7.8$ Hz, 2H). ^{13}C NMR (126 MHz, $DMSO-d_6$) δ 162.64, 160.09, 153.49, 144.56, 135.79, 135.15, 127.01, 125.12, 125.00, 123.28, 119.33, 116.96, 112.88, 111.62, 108.81, 38.58, 23.59, 21.66. HPLC purity: 100%. HRMS (ESI): m/z calculated for $C_{18}H_{17}N_6$ $[M + H]^+$: 317.1515. Found: 317.1522.

11-(1-Methyl-1H-pyrazol-4-yl)-5,6,7,8-tetrahydropyrimido[4',5':3,4]cyclohepta[1,2-b]indol-2-amine (13). The reaction was carried out according to general procedure F using **43** (199 mg, 0.60 mmol), (1-methyl-1H-pyrazol-4-yl)boronic acid (189 mg, 0.90 mmol), K_2CO_3 (167 mg, 1.21 mmol), and $Pd(PPh_3)_4$ (35 mg, 30 μ mol) in a mixture of dioxane/water (2.0 mL/0.3 mL) at 95 °C overnight to afford the title compound (29 mg, 15% yield). 1H NMR (500 MHz, $DMSO-d_6$) δ 11.42 (s, 1H), 8.88 (s, 1H), 8.15 (s, 1H), 7.91 (d, $J = 11.0$ Hz, 2H), 7.31 (d, $J = 8.1$ Hz, 1H), 7.24 (d, $J = 8.3$ Hz, 1H), 6.29 (s, 2H), 3.87 (s, 3H), 3.16 (t, $J = 6.5$ Hz, 2H), 2.65–2.59 (m, 2H), 1.94 (dt, $J = 11.8, 6.5$ Hz, 2H). ^{13}C NMR (126 MHz, $DMSO-d_6$) δ 162.04, 161.38, 156.59, 143.50, 135.91, 134.77, 128.05, 127.14, 124.45, 123.60, 119.88, 119.53, 119.40, 110.42, 110.40, 38.53, 30.05, 29.72, 23.96. HPLC purity: 100%. HRMS (ESI): m/z calculated for $C_{19}H_{19}N_6$ $[M + H]^+$: 331.1671. Found: 331.1661.

12-Cyclopropyl-6,7,8,9-tetrahydro-5H-pyrimido[4',5':3,4]-cycloocta[1,2-b]indol-2-amine (30). A mixture of **44** (226 mg, 0.66 mmol), cyclopropylboronic acid (395 mg, 4.6 mmol), and K_3PO_4 (697 mg, 3.3 mmol) in dioxane (10 mL) was degassed, followed by the addition of $Pd(dppf)Cl_2$ (27 mg, 33 μ mol). The reaction mixture was heated to 80 °C and allowed to stir overnight. After completion of the reaction, the mixture was cooled to r.t. and diluted with EtOAc and water. The organic layer was washed with water and concentrated *in vacuo*. The crude residue was purified via preparative HPLC to afford the title compound (7.9 mg, 4.0% yield). 1H NMR (850 MHz, CD_3OD-d_4) δ 8.08 (s, 1H), 7.56 (d, $J = 1.7$ Hz, 1H), 7.18 (dd, $J = 8.3, 0.6$ Hz, 1H), 6.87 (dd, $J = 8.3, 1.7$ Hz, 1H), 3.04–2.99 (m, 2H), 2.63 (s, 2H), 1.99–1.93 (m, 1H), 1.86–1.81 (m, 4H), 0.90–0.85 (m, 2H), 0.66–0.63 (m, 2H). ^{13}C NMR (214 MHz, CD_3OD-d_4) δ 165.96, 162.18, 157.95, 142.89, 136.61, 136.04, 129.23, 122.97, 121.39, 117.73, 111.21, 109.69, 32.33, 29.00, 28.29, 22.52, 16.47, 8.95. HPLC purity: 100%. HRMS (ESI): m/z calculated for $C_{19}H_{21}N_4$ $[M + H]^+$: 305.1766. Found: 305.1757.

Biological Evaluation: Kinome Screening. The Eurofins DiscoverX Corporation *scanMAX* assay platform was employed to assess the selectivity of each final compound at a single concentration of 1 μ M. The *scanMAX* assay platform profiles a compound against 403 wild-type (WT) human kinases and produces percent of control (PoC) values.⁴⁸ A selectivity score can be calculated using the PoC values. Selectivity scores ($S_{10}(1 \mu M)$) are included in Tables 1–4 as well as the number of WT human kinases in the *scanMAX* panel with PoC < 10. Kinome tree diagrams as well as tables of potentially inhibited kinases in this screen for analogues **8**, **17**, and **30** are included in Figure S1. K_d determination using the DiscoverX PIP4K2C assay was carried out for analogue **17** and included in Table S3.

Enzymatic Assays. SignalChem developed an ADP-Glo assay (Promega) to evaluate the enzymatic inhibition of PIKfyve by several compounds in Tables 1–4, S1, and S3. The assay was optimized to give a high signal-to-noise ratio, which involved using 25 ng/reaction of PIKfyve protein prepared by SignalChem (Catalog No. P17-31G), 0.1 μ g/ μ L PI(3)P:PS as the substrate, and 25 μ M ATP, as suggested by the manufacturer's protocol. This concentration of ATP is well above the K_m value for ATP for PIKfyve, published as 9.9 μ M.⁴⁹ The assay was run with a 60-min incubation of the components at r.t. Executing the

assay in dose–response (10-pt curve) in duplicate allowed for the calculation of IC_{50} values.

Eurofins enzymatic radiometric assays were run at the K_m value for ATP using a single concentration (1 μ M) in duplicate to produce PoC values for each kinase listed in Table S2. The same assay format, also executed at the K_m value for ATP, was used to generate dose–response (9-pt) curves for several kinases listed in Tables S1 and S3. The substrate used, protein constructs, controls, and assay protocol for these enzymatic radiometric kinase assays can be found on the Eurofins website: <https://www.eurofinsdiscoveryservices.com>.

Several Reaction Biology Corp. (RBC) radiometric HotSpot kinase assays were carried out at the K_m value for ATP in dose–response (10-pt curve), specifically for MYLK4, RIPK5, and YSK4. The corresponding IC_{50} values are included in Tables S1 and S3. Details related to the substrate used, protein constructs, controls, and assay protocol for these HotSpot kinase assays can be accessed via the RBC website: <https://www.reactionbiology.com/list-kinase-targets-us-facility>.

NanoBRET Assays. Human embryonic kidney (HEK293) cells (hypotriploid, female, fetal) obtained from ATCC were cultured in Dulbecco's Modified Eagle's medium (DMEM, Gibco) supplemented with 10% (v/v) fetal bovine serum (FBS, Corning). These cells were incubated in 5% CO_2 at 37 °C and passaged every 72 h with trypsin (Gibco), ensuring that they never reached confluency.

Constructs for NanoBRET measurements of PIKfyve (PIKfyve-NLuc), PISP4K γ (PISP4K γ -NLuc), MAP4K5 (MAP4K5-NLuc), and MYLK4 (MYLK4-NLuc) included in Tables 1–5, S1, and S3 were kindly provided by Promega. The NLuc orientations used in the respective assays are indicated in parentheses after each construct. The NanoBRET assays were executed in dose–response (12-pt curves) as described previously.^{50,51} Assays were carried out as described by the manufacturer using 0.13 μ M tracer K8 for PIKfyve, 0.063 μ M tracer K8 for PISP4K γ , 1 μ M tracer K10 for MAP4K5, and 0.13 μ M tracer K10 for MYLK4. Representative curves generated for PIKfyve are included in Figure S1 and for MYLK and MAP4K5 versus compound **17** in Figure S2. The NanoBRET data for TYK2 (JH2 domain-pseudokinase) included in Table S1 was generated by RBC.

Kinetic Solubility. Analiza, Inc. analyzed the kinetic solubility of a 10 mM DMSO stock solution of compound **17** dissolved in phosphate buffered saline (PBS) solution at pH 7.4 as described previously.¹⁷ The reported solubility value has been corrected for background nitrogen present in the media and DMSO.

Microsomal Stability Analysis. Analiza, Inc. analyzed the microsomal stability using a 10 mM DMSO stock solution of compound **17**, which was diluted upon arrival to 0.5 mM with DMSO and again to 0.1 mM with acetonitrile (ACN). The resulting solution contained 0.1 mM of compound **17** in 20% DMSO/80% ACN. Microsomes were isolated from male (CD-1) mice and supplied at a 20 mg/mL protein concentration. For the assay, the reaction plate was prepared by treating a prewarmed (37 °C) microsomal solution (0.63 mg/mL protein in 100 mM KPO_4 with 1.3 mM ethylenediamine tetraacetic acid (EDTA)) with 0.1 mM compound or reference standard and mixing thoroughly by repeated pipetting. The resulting solution was preincubated for 5 min at 37 °C before preparing the $T = 0$ plates. The $T = 0$ plate was prepared to include an aliquot of the reaction plate, diluted with cold (4 °C) MeOH, and mixed thoroughly by repeated pipetting and treated with nicotinamide adenine dinucleotide phosphate (NADPH) regeneration solution with mixing via repeated pipetting. The $T = 30$ incubation plate was prepared by adding NADPH to the reaction plate, sealing, and incubating at 37 °C for 30 min and then transferring an aliquot to a fresh plate and quenching the reaction with cold (4 °C) MeOH. Prior to analysis, all plates were sealed, vortexed, and centrifuged at 3000 RPM at 4 °C for 15 min, and the supernatants analyzed by liquid chromatography time-of-flight mass spectrometry (LC-TOFMS) (AQUASIL C18 column, eluting with a fast generic gradient program). TOFMS data was acquired using Agilent 6538 Ultra High Accuracy TOFMS in extended dynamic range (m/z 100–1000) using generic MS conditions in positive mode. Following data acquisition, exact mass extraction and peak integration was performed using MassHunter Software (Agilent Technologies).

Compound stability was calculated as the percent remaining of the unchanged parent compound at 30 min ($T = 30$) relative to the peak area at $T = 0$. On-board reference standards were within the acceptable range for the assay and correlated to reported values, ensuring the quality of the assay.

MHV-nLuc Assay. Murine astrocytoma delayed brain-tumor (DBT) cells were cultured at 37 °C in DMEM (Sigma) supplemented with 10% FBS (Gibco) with penicillin and streptomycin (Sigma) added.

The MHV-nLuc virus was engineered as described previously.²⁵ Next, MHV-nLuc virus stocks were grown on DBT cells and the 50% tissue culture infectious dose (TCID₅₀) assay employed to determine their titers. To run the MHV-nLuc assay, DBT cells were plated in 96-well plates at 80% confluency. PIKfyve inhibitors were diluted in DMEM, preparing 4-fold serial dilutions over a concentration range of 15–0.22 μM. The assay protocol was executed as previously described.²⁵ An LDH assay was run in parallel to assess the viability (Figure S3).²⁵ Three biological replicates each with three technical replicates were analyzed using GraphPad Prism to generate the IC₅₀ values included in Table 5 and graph in Figure 4A. These were then converted to pIC₅₀ values for Figure 4. Individual replicates for Figure 4A are included in Figure S4.

SARS-CoV-2-nLuc Assay. Human epithelial A549-ACE2 cells were cultured at 37 °C with 5% CO₂ in DMEM supplemented with 10% heat-inactivated FBS, nonessential amino acids, penicillin, and streptomycin. The ic-SARS-CoV-2-nLuc virus was engineered and prepared as described previously.²⁷ PIKfyve inhibitors and remdesivir (positive control) were diluted in DMEM, preparing 4-fold serial dilutions over a concentration range from 10 to 0.0006 μM. The assay protocol was executed in dose–response (8-point curve) as previously described ($n = 4$, with two technical replicates per assay).²⁷ Briefly, 1 day prior to infection, A549-ACE2 cells were seeded at 20 000 cells per well in 96-well solid black plates. On the day of infection, cells were pretreated with the compound for 1 h prior to infection. Next, ic-SARS-CoV-2-nLuc virus stocks were used to infect A549-ACE2 cells (85–95% confluent) at MOI = 0.02 for 2 h at 37 °C with 5% CO₂ with compound treatment maintained during the infection period. After 2 h, the supernatant was removed, infected monolayers rinsed with PBS, and media-containing compound added to each well. At 46 h post-infection, Nano-Glo reagent (Promega) was added to each well according to the manufacturer's protocol (Promega) and relative light units (RLUs) were measured using a Promega GloMax plate reader. An LDH assay to assess viability ($n = 2$, with two technical replicates per assay) was run in parallel using 20 000 uninfected A549-ACE2 cells per well in 96-well clear plates.²⁵ After 46 h of treatment with compounds in dose–response, an aliquot of the supernatant from each well was taken, centrifuged to remove cell and debris, and transferred to a clean plate. The clarified supernatant was stored frozen until analysis using the Sigma Tox7 kit according to the manufacturer's protocol. Data was analyzed using GraphPad Prism to generate the graphs and IC₅₀ values included in Figures 4 and S5 and Table 5, respectively.

Spike Uptake Assay in HEK293T-ACE2 Cells. The protocol employed to measure and quantify the uptake of spike protein was previously described.^{25,37} Briefly, HEK293T-ACE2 cells were seeded onto poly-L-lysine-treated coverslips and allowed to adhere for 24 h at 37 °C. Next, 1 h prior to the addition of spike protein, cell media was changed to starvation media (lacking serum) supplemented with either 1 μM test compound or DMSO (vehicle control). After addition of His6-SARS-CoV-2 spike protein (5 μg per well) to each coverslip, cells were incubated at 0 °C (on ice) for 30 min. Cells were next washed with PBS and fresh starvation media supplemented with either the same test compound at 1 μM or DMSO, followed by a final incubation for 30 min at 37 °C. Prior to fixation, cells were washed for 60 s and then rinsed with acid to remove any extracellular spike protein. Next, cells were washed with PBS and fixed for 10 min with paraformaldehyde at 4 °C. Cells were then permeabilized in 0.2% Triton X-100 in PBS and blocked with 5% bovine serum albumin (BSA). His-tag antibody (HIS.H8) conjugated with Dylight 550 (ThermoFisher) was used to visualize and quantify spike protein uptake. Imaging of cells was executed using a Leica TCS SP8 confocal microscope. Quantification

was carried out using Leica LAS X software, with statistical calculations and graphs produced using Prism GraphPad software. Quantification of fluorescence per cell was not necessary since HEK293T-ACE2 cells were at full confluency, resulting in approximately an equal number of cells per field. Statistics were carried out.

Spike Uptake Assay in Calu-3 and Caco-2 Cells. To measure and quantify the uptake of spike protein, the original protocol employed with HEK293T-ACE2 cells was modified.^{25,37} Calu-3 and Caco-2 were seeded as single cells on poly-D-lysine-treated coverslips and allowed to adhere for 36 h at 37 °C. Seeding as single cells allowed for reduced clustering and cyst formation of Caco-2 cells and allowed for clear separation between Calu-3 cells. Cells were grown in ATCC-formulated Eagle's minimum essential medium (Catalog No. 30-2003) supplemented with 20% FBS. Next, 2 h prior to the addition of His6-SARS-CoV-2 spike protein, cell media was changed to starvation media (lacking serum) supplemented with either 1 μM test compound or DMSO (vehicle control). Following addition of spike protein (5 μg per well) to each coverslip, cells were incubated at 0 °C (on ice) for 30 min. Cells were next washed with PBS and fresh starvation media supplemented with either 1 μM test compound or DMSO, followed by a final 1 h incubation at 37 °C. Prior to fixation, cells were rinsed for 90 s with acid wash solution (pH = 3.0) to wash away any residual extracellular spike protein. Next, cells were washed with PBS and fixed for 10 min with paraformaldehyde at 4 °C. Cells were then permeabilized in a solution of 0.2% Triton X-100 in PBS and blocked with 5% BSA. A combination of His-tag primary antibody (HIS.H8, ThermoFisher) with Alexa Fluor 488 secondary antibody (ThermoFisher) was used to visualize and quantify spike protein uptake. Cells were imaged using a Leica TCS SP8 confocal microscope and quantification was carried out using Leica LAS X software. Statistical calculations and graphs were produced using Prism GraphPad software. For these studies, the number of cells was factored into the quantification of fluorescence: fluorescence intensity was divided by the number of nuclei in each image. This method accounted for the variable number of cells.

Lentivirus Uptake Assay. Calu-3 cells were seeded at ~100 000 cells per well (24-well plate) on poly-L-lysine-treated coverslips. At 96 h after seeding, cells were incubated with 1 μM of each compound (or DMSO) for 1 h. Subsequently, pseudovirus SARS-CoV-2 (Catalog No. 78010, BPS Biosciences Inc., Figure 7) or bald GFP lentivirus (Catalog no. 79987, BPS Biosciences Inc., Figure S6) was added to cells for 12 h. After this incubation, virus-containing media was replaced with fresh DMEM media and incubated further for 48 h. Cells were fixed with 4% paraformaldehyde for 20 min at 4 °C and stained with Hoechst. Cells treated with the pseudovirus were then permeabilized, blocked, and stained using Spike antibody (GTX632604) and conjugated with Alexa Fluor 488 (ThermoFisher). Cells were imaged using a Leica TCS SP8 confocal microscope. To quantify the results, nuclei and GFP/Alexa Fluor fluorescing cells were counted using the "Find Maxima" function in ImageJ. GFP/Alexa Fluor counts were then divided by nuclei count for every image. The percentage of infected cells for each image was calculated and analyzed using one-way ANOVA and post-hoc Tukey test.

Lysosomal Staining Protocol. Human neuroblastoma (SH-SY5Y) cells obtained from ATCC were cultured in Dulbecco's Modified Eagle Medium/Nutrient Mixture F12 medium (DMEM/F12, Gibco) supplemented with 10% (v/v) fetal bovine serum (FBS, Corning). SH-SY5Y cells were incubated in 5% CO₂ at 37 °C and passaged every 48 h with trypsin (Gibco).

SH-SY5Y cells were plated in 35 mm glass bottom dishes and treated for 24 h with either 0.05% DMSO (control) or 5 μM of the indicated compound. After 24 h, 50 nM LysoTracker Red DND-99 (ThermoFisher) was added to each dish. The dishes were incubated for 30 min at 37 °C. Live cells were imaged at 40× magnification. Quantification of fluorescence was performed using ImageJ. Mean intensity of the LysoTracker fluorescence was calculated from five regions per image. Mean intensity was normalized to cell number within each region. Bar graph (Figure S7) represents the average LysoTracker fluorescence ($n = 2$). Error bars represent the standard deviation.

■ ASSOCIATED CONTENT

SI Supporting Information

The Supporting Information is available free of charge at <https://pubs.acs.org/doi/10.1021/acs.jmedchem.2c00697>.

Molecular formula strings (CSV)

Comprehensive profiling of analogues **8** and **17**, an additional figure that details kinome-wide selectivity of probe candidates **8** and **17** as well as negative control **30**, cell viability data in DBT cells, SARS-CoV-2 replication versus viability graphs, purity chromatograms, and NMR spectra (PDF)

■ AUTHOR INFORMATION

Corresponding Author

Alison D. Axtman – Structural Genomics Consortium, UNC Eshelman School of Pharmacy, University of North Carolina at Chapel Hill, Chapel Hill, North Carolina 27599, United States; orcid.org/0000-0003-4779-9932; Email: alison.axtman@unc.edu

Authors

David H. Drewry – Structural Genomics Consortium, UNC Eshelman School of Pharmacy, University of North Carolina at Chapel Hill, Chapel Hill, North Carolina 27599, United States; UNC Lineberger Comprehensive Cancer Center, School of Medicine, University of North Carolina at Chapel Hill, Chapel Hill, North Carolina 27599, United States; orcid.org/0000-0001-5973-5798

Frances M. Potjewyd – Structural Genomics Consortium, UNC Eshelman School of Pharmacy, University of North Carolina at Chapel Hill, Chapel Hill, North Carolina 27599, United States; orcid.org/0000-0003-4241-9873

Armin Bayati – Structural Genomics Consortium, Department of Neurology and Neurosurgery, Montreal Neurological Institute, McGill University, Montreal, QC H3A 2B4, Canada

Jeffery L. Smith – Structural Genomics Consortium, UNC Eshelman School of Pharmacy, University of North Carolina at Chapel Hill, Chapel Hill, North Carolina 27599, United States; orcid.org/0000-0003-2189-0420

Rebekah J. Dickmader – UNC Lineberger Comprehensive Cancer Center, School of Medicine, Department of Microbiology & Immunology, and Department of Chemistry, University of North Carolina at Chapel Hill, Chapel Hill, North Carolina 27599, United States; Rapidly Emerging Antiviral Drug Development Initiative (READDI), Chapel Hill, North Carolina 27599, United States

Stefanie Howell – Structural Genomics Consortium, UNC Eshelman School of Pharmacy, University of North Carolina at Chapel Hill, Chapel Hill, North Carolina 27599, United States

Sharon Taft-Benz – Rapidly Emerging Antiviral Drug Development Initiative (READDI), Chapel Hill, North Carolina 27599, United States; Department of Genetics, University of North Carolina at Chapel Hill, Chapel Hill, North Carolina 27599, United States

Sophia M. Min – Structural Genomics Consortium, UNC Eshelman School of Pharmacy, University of North Carolina at Chapel Hill, Chapel Hill, North Carolina 27599, United States; orcid.org/0000-0001-9840-2996

Mohammad Anwar Hossain – Structural Genomics Consortium, UNC Eshelman School of Pharmacy, University

of North Carolina at Chapel Hill, Chapel Hill, North Carolina 27599, United States; orcid.org/0000-0001-8684-8755

Mark Heise – Rapidly Emerging Antiviral Drug Development Initiative (READDI), Chapel Hill, North Carolina 27599, United States; Department of Genetics, University of North Carolina at Chapel Hill, Chapel Hill, North Carolina 27599, United States

Peter S. McPherson – Structural Genomics Consortium, Department of Neurology and Neurosurgery, Montreal Neurological Institute, McGill University, Montreal, QC H3A 2B4, Canada

Nathaniel J. Moorman – UNC Lineberger Comprehensive Cancer Center, School of Medicine and Department of Microbiology & Immunology, University of North Carolina at Chapel Hill, Chapel Hill, North Carolina 27599, United States; Rapidly Emerging Antiviral Drug Development Initiative (READDI), Chapel Hill, North Carolina 27599, United States

Complete contact information is available at:

<https://pubs.acs.org/10.1021/acs.jmedchem.2c00697>

Author Contributions

[○]D.H.D. and F.M.P. contributed equally to this work. All authors have given approval to the final version of the manuscript.

Notes

The authors declare no competing financial interest.

■ ACKNOWLEDGMENTS

Constructs for NanoBRET measurements of PIKfyve and PISP4Ky were kindly provided by Promega. The authors thank SignalChem Biotech Inc. for helping to enable and optimize an enzymatic assay for profiling our compounds against PIKfyve. The TREEspot kinase interaction mapping software was employed in preparation of the kinome trees in [Figure S1: <http://treespot.discoverx.com>](#). The table of contents graphic was created with Biorender.com. The authors also thank ChemSpace for synthetic support. The authors acknowledge the Department of Chemistry Mass Spectrometry Core Laboratory at the University of North Carolina for their assistance with mass spectrometry experiments. The Structural Genomics Consortium is a registered charity (number 1097737) that receives funds from AbbVie, Bayer Pharma AG, Boehringer Ingelheim, Canada Foundation for Innovation, Eshelman Institute for Innovation, Genome Canada, Genentech, Innovative Medicines Initiative (EU/EFPIA), Janssen, Merck KGaA Darmstadt Germany, MSD, Novartis Pharma AG, Ontario Ministry of Economic Development and Innovation, Pfizer, São Paulo Research Foundation-FAPESP, Takeda, and Wellcome. Research reported in this publication was supported in part by the NC Biotechnology Center Institutional Support Grant 2018-IDG-1030, NIH U24DK116204. This project was supported by the Rapidly Emerging Antiviral Drug Development Initiative at the University of North Carolina at Chapel Hill with funding from the North Carolina Coronavirus State and Local Fiscal Recovery Funds program, appropriated by the North Carolina General Assembly.

■ ABBREVIATIONS USED

ACN, acetonitrile; ACE2, angiotensin-converting enzyme 2; AcOH, acetic acid; BSA, bovine serum albumin; DDQ, 2,3-dichloro-5,6-dicyano-1,4-benzoquinone; DIPA, *N,N*-diisopro-

pylamine; DMA, *N,N*-dimethylacetamide; DMF, *N,N*-dimethylformamide; DMSO, dimethyl sulfoxide; EtOAc, ethyl acetate; HPLC, high-performance liquid chromatography; IC₅₀, half-maximal inhibitory concentration; IPA, isopropylamine; K_m, Michaelis constant; LC-MS, liquid chromatography-mass spectrometry; MTBE, methyl *tert*-butyl ether; NanoBRET, bioluminescence resonance energy transfer using NanoLuciferase; NaOMe, sodium methoxide; nLuc, nanoLuciferase; NMR, nuclear magnetic resonance; TEA, triethylamine; TFA, trifluoroacetic acid; THF, tetrahydrofuran; SAR, structure–activity relationships; v/v, volume for volume

REFERENCES

- (1) Shisheva, A. PIKfyve: Partners, significance, debates and paradoxes. *Cell Biol. Int.* **2008**, *32*, 591–604.
- (2) Gayle, S.; Landrette, S.; Beeharry, N.; Conrad, C.; Hernandez, M.; Beckett, P.; Ferguson, S. M.; Mandelkern, T.; Zheng, M.; Xu, T.; Rothberg, J.; Lichenstein, H. Identification of apilimod as a first-in-class PIKfyve kinase inhibitor for treatment of B-cell non-Hodgkin lymphoma. *Blood* **2017**, *129*, 1768–1778.
- (3) Cai, X.; Xu, Y.; Cheung, A. K.; Tomlinson, R. C.; Alcázar-Román, A.; Murphy, L.; Billich, A.; Zhang, B.; Feng, Y.; Klumpp, M.; Rondeau, J.-M.; Fazal, A. N.; Wilson, C. J.; Myer, V.; Joberty, G.; Bouwmeester, T.; Labow, M. A.; Finan, P. M.; Porter, J. A.; Ploegh, H. L.; Baird, D.; De Camilli, P.; Tallarico, J. A.; Huang, Q. PIKfyve, a class III PI kinase, is the target of the small molecular IL-12/IL-23 inhibitor apilimod and a player in Toll-like receptor signaling. *Chem. Biol.* **2013**, *20*, 912–921.
- (4) Krausz, S.; Boumans, M. J.; Gerlag, D. M.; Lufkin, J.; van Kuijk, A. W.; Bakker, A.; de Boer, M.; Lodde, B. M.; Reedquist, K. A.; Jacobson, E. W.; O'Meara, M.; Tak, P. P. Brief report: A phase IIa, randomized, double-blind, placebo-controlled trial of apilimod mesylate, an interleukin-12/interleukin-23 inhibitor, in patients with rheumatoid arthritis. *Arthritis Rheum.* **2012**, *64*, 1750–1755.
- (5) Sands, B. E.; Jacobson, E. W.; Sylwestrowicz, T.; Younes, Z.; Dryden, G.; Fedorak, R.; Greenbloom, S. Randomized, double-blind, placebo-controlled trial of the oral interleukin-12/23 inhibitor apilimod mesylate for treatment of active Crohn's disease. *Inflammatory Bowel Dis.* **2010**, *16*, 1209–1218.
- (6) Baranov, M. V.; Bianchi, F.; van den Bogaart, G. The PIKfyve inhibitor apilimod: A double-edged sword against COVID-19. *Cells* **2021**, *10*, 30.
- (7) Kang, Y.-L.; Chou, Y.-y.; Rothlauf, P. W.; Liu, Z.; Soh, T. K.; Cureton, D.; Case, J. B.; Chen, R. E.; Diamond, M. S.; Whelan, S. P. J.; Kirchhausen, T. Inhibition of PIKfyve kinase prevents infection by Zaire ebolavirus and SARS-CoV-2. *Proc. Natl. Acad. Sci. U.S.A.* **2020**, *117*, 20803–20813.
- (8) Ikononov, O. C.; Sbrissa, D.; Shisheva, A. YM201636, an inhibitor of retroviral budding and PIKfyve-catalyzed PtdIns(3,5)P₂ synthesis, halts glucose entry by insulin in adipocytes. *Biochem. Biophys. Res. Commun.* **2009**, *382*, 566–570.
- (9) Hou, J.-Z.; Xi, Z.-Q.; Niu, J.; Li, W.; Wang, X.; Liang, C.; Sun, H.; Fang, D.; Xie, S.-Q. Inhibition of PIKfyve using YM201636 suppresses the growth of liver cancer via the induction of autophagy. *Oncol. Rep.* **2019**, *41*, 1971–1979.
- (10) Martin, S.; Harper, C. B.; May, L. M.; Coulson, E. J.; Meunier, F. A.; Osborne, S. L. Inhibition of PIKfyve by YM-201636 dysregulates autophagy and leads to apoptosis-independent neuronal cell death. *PLoS One* **2013**, *8*, No. e60152.
- (11) Jefferies, H. B. J.; Cooke, F. T.; Jat, P.; Boucheron, C.; Koizumi, T.; Hayakawa, M.; Kaizawa, H.; Ohishi, T.; Workman, P.; Waterfield, M. D.; Parker, P. J. A selective PIKfyve inhibitor blocks PtdIns(3,5)-P(2) production and disrupts endomembrane transport and retroviral budding. *EMBO Rep.* **2008**, *9*, 164–170.
- (12) Soares, A. C.; Ferreira, A.; Mariën, J.; Delay, C.; Lee, E.; Trojanowski, J. Q.; Moechars, D.; Annaert, W.; De Muyneck, L. PIKfyve activity is required for lysosomal trafficking of tau aggregates and tau seeding. *J. Biol. Chem.* **2021**, *296*, No. 100636.
- (13) de Campos, C. B.; Zhu, Y. X.; Sepetov, N.; Romanov, S.; Bruins, L. A.; Shi, C. X.; Stein, C. K.; Petit, J. L.; Polito, A. N.; Sharik, M. E.; Meermeier, E. W.; Ahmann, G. J.; Armenta, I. D. L.; Kruse, J.; Bergsagel, P. L.; Chesi, M.; Meurice, N.; Braggio, E.; Stewart, A. K. Identification of PIKfyve kinase as a target in multiple myeloma. *Haematologica* **2020**, *105*, 1641–1649.
- (14) Hayakawa, N.; Noguchi, M.; Takeshita, S.; Eviyanti, A.; Seki, Y.; Nishio, H.; Yokoyama, R.; Noguchi, M.; Shuto, M.; Shima, Y.; Kuribayashi, K.; Kageyama, S.; Eda, H.; Suzuki, M.; Hatta, T.; Iemura, S.-I.; Natsume, T.; Tanabe, I.; Nakagawa, R.; Shiozaki, M.; Sakurai, K.; Shoji, M.; Andou, A.; Yamamoto, T. Structure-activity relationship study, target identification, and pharmacological characterization of a small molecular IL-12/23 inhibitor, APY0201. *Bioorg. Med. Chem.* **2014**, *22*, 3021–3029.
- (15) Andrs, M.; Korabecny, J.; Jun, D.; Hodny, Z.; Bartek, J.; Kuca, K. Phosphatidylinositol 3-kinase (PI3K) and phosphatidylinositol 3-kinase-related kinase (PIKK) inhibitors: Importance of the morpholine ring. *J. Med. Chem.* **2015**, *58*, 41–71.
- (16) Lees, J. A.; Li, P.; Kumar, N.; Weisman, L. S.; Reinisch, K. M. Insights into lysosomal PI(3,5)P(2) homeostasis from a structural-biochemical analysis of the PIKfyve lipid kinase complex. *Mol. Cell* **2020**, *80*, 736–743.e734.
- (17) Drewry, D. H.; Annor-Gyamfi, J. K.; Wells, C. I.; Pickett, J. E.; Dederer, V.; Preuss, F.; Mathea, S.; Axtman, A. D. Identification of pyrimidine-based lead compounds for understudied kinases implicated in driving neurodegeneration. *J. Med. Chem.* **2022**, *65*, 1313–1328.
- (18) Eduful, B. J.; O'Byrne, S. N.; Temme, L.; Asquith, C. R. M.; Liang, Y.; Picado, A.; Pilote, J. R.; Hossain, M. A.; Wells, C. I.; Zuercher, W. J.; Catta-Preta, C. M. C.; Ramos, P. Z.; Santiago, A. D. S.; Couñago, R. M.; Langendorf, C. G.; Nay, K.; Oakhill, J. S.; Pulliam, T. L.; Lin, C.; Awad, D.; Willson, T. M.; Frigo, D. E.; Scott, J. W.; Drewry, D. H. Hinge binder scaffold hopping identifies potent calcium/calmodulin-dependent protein kinase kinase 2 (CAMKK2) inhibitor chemotypes. *J. Med. Chem.* **2021**, *64*, 10849–10877.
- (19) Sharma, V.; Gupta, M. Designing of kinase hinge binders: A medicinal chemistry perspective. *Chem. Biol. Drug Des.* **2022**, *14024* DOI: 10.1111/cbdd.14024.
- (20) Jia, C.-C.; Chen, W.; Feng, Z.-L.; Liu, Z.-P. Recent developments of RET protein kinase inhibitors with diverse scaffolds as hinge binders. *Future Med. Chem.* **2021**, *13*, 45–62.
- (21) Halkina, T.; Henderson, J. L.; Lin, E. Y.; Himmelbauer, M. K.; Jones, J. H.; Nevalainen, M.; Feng, J.; King, K.; Rooney, M.; Johnson, J. L.; Marcotte, D. J.; Chodaparambil, J. V.; Kumar, P. R.; Patterson, T. A.; Murugan, P.; Schuman, E.; Wong, L.; Hesson, T.; Lamore, S.; Bao, C.; Calhoun, M.; Certo, H.; Amaral, B.; Dillon, G. M.; Gilfillan, R.; de Turiso, F. G. Discovery of potent and brain-penetrant tau tubulin kinase 1 (TTBK1) inhibitors that lower tau phosphorylation in vivo. *J. Med. Chem.* **2021**, *64*, 6358–6380.
- (22) Potjewy, F. M.; Marquez, A. B.; Chaikuad, A.; Howell, S.; Dunn, A. S.; Beltran, A. A.; Smith, J. L.; Drewry, D. H.; Beltran, A. S.; Axtman, A. D. Modulation of tau tubulin kinases (TTBK1 and TTBK2) impacts ciliogenesis. *bioRxiv* **2022**, 2022.2005.2006.490937. DOI: 10.1101/2022.05.06.490937.
- (23) Asquith, C. R. M.; Berger, B.-T.; Wan, J.; Bennett, J. M.; Capuzzi, S. J.; Crona, D. J.; Drewry, D. H.; East, M. P.; Elkins, J. M.; Fedorov, O.; Godoi, P. H.; Hunter, D. M.; Knapp, S.; Müller, S.; Torrice, C. D.; Wells, C. I.; Earp, H. S.; Willson, T. M.; Zuercher, W. J. SGC-GAK-1: A chemical probe for cyclin G associated kinase (GAK). *J. Med. Chem.* **2019**, *62*, 2830–2836.
- (24) Dillon, G. M.; Henderson, J. L.; Bao, C.; Joyce, J. A.; Calhoun, M.; Amaral, B.; King, K. W.; Bajrami, B.; Rabah, D. Acute inhibition of the CNS-specific kinase TTBK1 significantly lowers tau phosphorylation at several disease relevant sites. *PLoS One* **2020**, *15*, No. e0228771.
- (25) Yang, X.; Dickmander, R. J.; Bayati, A.; Taft-Benz, S. A.; Smith, J. L.; Wells, C. I.; Madden, E. A.; Brown, J. W.; Lenarcic, E. M.; Yount, B. L., Jr; Chang, E.; Axtman, A. D.; Baric, R. S.; Heise, M. T.; McPherson, P. S.; Moorman, N.; Willson, T. M. Host kinase CSNK2 is a target for

inhibition of pathogenic SARS-like β -coronaviruses. *ACS Chem. Biol.* **2022**, *17*, 1937–1950.

(26) Körner, R. W.; Majjouti, M.; Alcazar, M. A. A.; Mahabir, E. Of mice and men: The coronavirus MHV and mouse models as a translational approach to understand SAR-CoV-2. *Viruses* **2020**, *12*, 880.

(27) Hou, Y. J.; Okuda, K.; Edwards, C. E.; Martinez, D. R.; Asakura, T.; Dinnon, K. H.; Kato, T.; Lee, R. E.; Yount, B. L.; Mascenik, T. M.; Chen, G.; Olivier, K. N.; Ghio, A.; Tse, L. V.; Leist, S. R.; Gralinski, L. E.; Schäfer, A.; Dang, H.; Gilmore, R.; Nakano, S.; Sun, L.; Fulcher, M. L.; Livraghi-Butrico, A.; Nicely, N. I.; Cameron, M.; Cameron, C.; Kelvin, D. J.; de Silva, A.; Margolis, D. M.; Markmann, A.; Bartel, L.; Zumwalt, R.; Martinez, F. J.; Salvatore, S. P.; Borczuk, A.; Tata, P. R.; Sontake, V.; Kimple, A.; Jaspers, I.; O'Neal, W. K.; Randell, S. H.; Boucher, R. C.; Baric, R. S. SARS-CoV-2 reverse genetics reveals a variable infection gradient in the respiratory tract. *Cell* **2020**, *182*, 429–446.e414.

(28) Beigel, J. H.; Tomashek, K. M.; Dodd, L. E.; Mehta, A. K.; Zingman, B. S.; Kalil, A. C.; Hohmann, E.; Chu, H. Y.; Luetkemeyer, A.; Kline, S.; de Castilla, D. L.; Finberg, R. W.; Dierberg, K.; Tapon, V.; Hsieh, L.; Patterson, T. F.; Paredes, R.; Sweeney, D. A.; Short, W. R.; Touloumi, G.; Lye, D. C.; Ohmagari, N.; Oh, M.-D.; Ruiz-Palacios, G. M.; Benfield, T.; Fätkenheuer, G.; Kortepeter, M. G.; Atmar, R. L.; Creech, C. B.; Lundgren, J.; Babiker, A. G.; Pett, S.; Neaton, J. D.; Burgess, T. H.; Bonnett, T.; Green, M.; Makowski, M.; Osinusi, A.; Nayak, S.; Lane, H. C.; ACTT-1 Study Group Members. Remdesivir for the treatment of Covid-19 - Final report. *N. Engl. J. Med.* **2020**, *383*, 1813–1826.

(29) Nascimbeni, A. C.; Codogno, P.; Morel, E. Phosphatidylinositol-3-phosphate in the regulation of autophagy membrane dynamics. *FEBS J.* **2017**, *284*, 1267–1278.

(30) Marat, A. L.; Haucke, V. Phosphatidylinositol 3-phosphates at the interface between cell signalling and membrane traffic. *EMBO J.* **2016**, *35*, 561–579.

(31) Kreutzberger, A. J. B.; Sanyal, A.; Ojha, R.; Pyle, J. D.; Vapalahti, O.; Balistreri, G.; Kirchhausen, T.; Gallagher, T. Synergistic block of SARS-CoV-2 infection by combined drug inhibition of the host entry factors PIKfyve kinase and TMPRSS2 protease. *J. Virol.* **2021**, *95*, e00975–00921.

(32) Riva, L.; Yuan, S.; Yin, X.; Martin-Sancho, L.; Matsunaga, N.; Pache, L.; Burgstaller-Muehlbacher, S.; De Jesus, P. D.; Teriete, P.; Hull, M. V.; Chang, M. W.; Chan, J. F.-W.; Cao, J.; Poon, V. K.-M.; Herbert, K. M.; Cheng, K.; Nguyen, T.-T. H.; Rubanov, A.; Pu, Y.; Nguyen, C.; Choi, A.; Rathnasinghe, R.; Schotsaert, M.; Miorin, L.; Dejoze, M.; Zwaka, T. P.; Sit, K.-Y.; Martinez-Sobrido, L.; Liu, W.-C.; White, K. M.; Chapman, M. E.; Lendy, E. K.; Glynn, R. J.; Albrecht, R.; Rupp, E.; Mesecar, A. D.; Johnson, J. R.; Benner, C.; Sun, R.; Schultz, P. G.; Su, A. I.; Garcia-Sastre, A.; Chatterjee, A. K.; Yuen, K.-Y.; Chanda, S. K. Discovery of SARS-CoV-2 antiviral drugs through large-scale compound repurposing. *Nature* **2020**, *586*, 113–119.

(33) Xiu, S.; Dick, A.; Ju, H.; Mirzaie, S.; Abdi, F.; Cocklin, S.; Zhan, P.; Liu, X. Inhibitors of SARS-CoV-2 entry: Current and future opportunities. *J. Med. Chem.* **2020**, *63*, 12256–12274.

(34) Ribone, S. R.; Paz, S. A.; Abrams, C. F.; Villarreal, M. A. Target identification for repurposed drugs active against SARS-CoV-2 via high-throughput inverse docking. *J. Comput.-Aided Mol. Des.* **2022**, *36*, 25–37.

(35) Ou, X.; Liu, Y.; Lei, X.; Li, P.; Mi, D.; Ren, L.; Guo, L.; Guo, R.; Chen, T.; Hu, J.; Xiang, Z.; Mu, Z.; Chen, X.; Chen, J.; Hu, K.; Jin, Q.; Wang, J.; Qian, Z. Characterization of spike glycoprotein of SARS-CoV-2 on virus entry and its immune cross-reactivity with SARS-CoV. *Nat. Commun.* **2020**, *11*, No. 1620.

(36) Jackson, C. B.; Farzan, M.; Chen, B.; Choe, H. Mechanisms of SARS-CoV-2 entry into cells. *Nat Rev Mol Cell Biol* **2022**, *23*, 3–20.

(37) Bayati, A.; Kumar, R.; Francis, V.; McPherson, P. S. SARS-CoV-2 infects cells after viral entry via clathrin-mediated endocytosis. *J. Biol. Chem.* **2021**, *296*, No. 100306.

(38) Hoffmann, M.; Kleine-Weber, H.; Schroeder, S.; Krüger, N.; Herrler, T.; Erichsen, S.; Schiergens, T. S.; Herrler, G.; Wu, N.-H.;

Nitsche, A.; Müller, M. A.; Drosten, C.; Pöhlmann, S. SARS-CoV-2 cell entry depends on ACE2 and TMPRSS2 and is blocked by a clinically proven protease inhibitor. *Cell* **2020**, *181*, 271–280.e278.

(39) Mossel, E. C.; Huang, C.; Narayanan, K.; Makino, S.; Tesh, R. B.; Peters, C. J. Exogenous ACE2 expression allows refractory cell lines to support severe acute respiratory syndrome coronavirus replication. *J. Virol.* **2005**, *79*, 3846–3850.

(40) Koch, J.; Uckele, Z. M.; Doldan, P.; Stanifer, M.; Boulant, S.; Lozach, P. Y. TMPRSS2 expression dictates the entry route used by SARS-CoV-2 to infect host cells. *EMBO J.* **2021**, *40*, No. e107821.

(41) Dong, X. P.; Shen, D.; Wang, X.; Dawson, T.; Li, X.; Zhang, Q.; Cheng, X.; Zhang, Y.; Weisman, L. S.; Delling, M.; Xu, H. PI(3,5)P(2) controls membrane trafficking by direct activation of mucolipin Ca(2+) release channels in the endolysosome. *Nat. Commun.* **2010**, *1*, No. 38.

(42) Ikonov, O. C.; Sbrissa, D.; Mlak, K.; Kanzaki, M.; Pessin, J.; Shisheva, A. Functional dissection of lipid and protein kinase signals of PIKfyve reveals the role of PtdIns 3,5-P2 production for endomembrane integrity. *J. Biol. Chem.* **2002**, *277*, 9206–9211.

(43) Min, S. H.; Suzuki, A.; Stalker, T. J.; Zhao, L.; Wang, Y.; McKennan, C.; Riese, M. J.; Guzman, J. F.; Zhang, S.; Lian, L.; Joshi, R.; Meng, R.; Seeholzer, S. H.; Choi, J. K.; Koretzky, G.; Marks, M. S.; Abrams, C. S. Loss of PIKfyve in platelets causes a lysosomal disease leading to inflammation and thrombosis in mice. *Nat. Commun.* **2014**, *5*, No. 4691.

(44) Ravindran, M. S.; Bagchi, P.; Cunningham, C. N.; Tsai, B. Opportunistic intruders: How viruses orchestrate their functions to infect cells. *Nat. Rev. Microbiol.* **2016**, *14*, 407–420.

(45) Robinson, M.; Schor, S.; Barouch-Bentov, R.; Einav, S. Viral journeys on the intracellular highways. *Cell. Mol. Life Sci.* **2018**, *75*, 3693–3714.

(46) Ghosh, S.; Dellibovi-Ragheb, T. A.; Kerviel, A.; Pak, E.; Qiu, Q.; Fisher, M.; Takvorian, P. M.; Bleck, C.; Hsu, V. W.; Fehr, A. R.; Perlman, S.; Achar, S. R.; Straus, M. R.; Whittaker, G. R.; de Haan, C. A. M.; Kehrl, J.; Altan-Bonnet, G.; Altan-Bonnet, N. β -coronaviruses use lysosomes for egress instead of the biosynthetic secretory pathway. *Cell* **2020**, *183*, 1520–1535.e1514.

(47) Li, K.; McGee, L. R.; Fisher, B.; Sudom, A.; Liu, J.; Rubenstein, S. M.; Anwer, M. K.; Cushing, T. D.; Shin, Y.; Ayres, M.; Lee, F.; Eksterowicz, J.; Faulder, P.; Waszkowycz, B.; Plotnikova, O.; Farrelly, E.; Xiao, S.-H.; Chen, G.; Wang, Z. Inhibiting NF- κ B-inducing kinase (NIK): Discovery, structure-based design, synthesis, structure–activity relationship, and co-crystal structures. *Bioorg. Med. Chem. Lett.* **2013**, *23*, 1238–1244.

(48) Davis, M. I.; Hunt, J. P.; Herrgard, S.; Ciceri, P.; Wodicka, L. M.; Pallares, G.; Hocker, M.; Treiber, D. K.; Zarrinkar, P. P. Comprehensive analysis of kinase inhibitor selectivity. *Nat. Biotechnol.* **2011**, *29*, 1046–1051.

(49) Fogarty, K.; Kashem, M.; Bauer, A.; Bernardino, A.; Brennan, D.; Cook, B.; Farrow, N.; Molinaro, T.; Nelson, R. Development of three orthogonal assays suitable for the identification and qualification of PIKfyve inhibitors. *Assay Drug Dev. Technol.* **2017**, *15*, 210–219.

(50) Wells, C.; Couñago, R. M.; Limas, J. C.; Almeida, T. L.; Cook, J. G.; Drewry, D. H.; Elkins, J. M.; Gileadi, O.; Kapadia, N. R.; Lorentes-Macias, A.; Pickett, J. E.; Riemen, A.; Ruela-de-Sousa, R. R.; Willson, T. M.; Zhang, C.; Zuercher, W. J.; Zutshi, R.; Axtman, A. D. SGC-AAK1-1: A chemical probe targeting AAK1 and BMP2K. *ACS Med. Chem. Lett.* **2020**, *11*, 340–345.

(51) Wells, C. I.; Drewry, D. H.; Pickett, J. E.; Tjaden, A.; Krämer, A.; Müller, S.; Gyenis, L.; Menyhart, D.; Litchfield, D. W.; Knapp, S.; Axtman, A. D. Development of a potent and selective chemical probe for the pleiotropic kinase CK2. *Cell Chem. Biol.* **2021**, *28*, 546–558.e510.